Reproductive adaptation mechanism of female *Haemaphysalis longicornis* in response to transient extreme heat stress

AUTHORS

Feng-Jiao Li[1,2,#], Dan-Lin Qi[1,#], Jing-Ze Liu[1,*]

AFFILIATIONS

[1]Ministry of Education Key Laboratory of Molecular and Cellular Biology, Hebei Key Laboratory of Animal Physiology, Biochemistry and Molecular Biology, Hebei Research Center of the Basic Discipline of Cellular Biology, Hebei Collaborative Innovation Center for Eco-Environment, College of Life Sciences, Hebei Normal University, Shijiazhuang, Hebei 050024, China

[2]Postdoctoral Research Station in Ecology, College of Life Sciences, Hebei Normal University, Shijiazhuang, Hebei 050024, China

CORRESPONDING AUTHOR:

Jingze Liu: liujingze@hebtu.edu.cn; https://orcid.org/0000-0002-0923-1775

CONTRIBUTIONS

FL and JL designed the study. FL and DQ performed the experiments and prepared the data and figures. FL analyzed the data and wrote the manuscript. JL edited and reviewed the manuscript. All authors read and approved the manuscript.

ABSTRACT

Global climate change includes a substantial increase in the frequency and intensity of extreme high temperatures which pose a threat to the survival of arthropod individuals and populations. As a blood sucking arthropod, *Haemaphysalis longicornis* is mainly distributed in Asia with an expanding distribution range that has successfully invaded multiple regions, and has excellent ecological adaptability. In the natural environment, *H. longicornis* has the capacity of tolerating environment temperature of 5.7°C to 42.1°C. However, the heat stress response mechanism of *H. longicornis* has not been revealed. In order to illustrate the heat stress tolerance and ecological adaptability of *H. longicornis*, we exposed the engorged female ticks to transient extreme heat (42°C for 30 min), and found that the heat stress did not affect the survival of engorged females, and had only limited effects on reproduction. Based on the microbiome, metabolome and transcriptome analyses, it was confirmed that *H. longicornis* has a series of complex and efficient heat stress repair mechanisms. Among them, the obligate endosymbiotic bacteria that *Coxiella*-like endosymbiotic of *H. longicornis* (CLE-Hl) and the *heat shock protein 68* (*Hsp68*) gene play an important role in heat stress tolerance of *H. longicornis*. In summary, this study uncovers details for understanding the heat stress tolerance mechanism from multiaspects, and further confirms that *H. longicornis* has excellent ecological adaptability.

KEY WORDS

Haemaphysalis longicornis; Short-term high temperature stress; *16S rRNA*; Transcriptome; Metabolome

INTRODUCTION

Ticks, a blood sucking arthropod, are widely distributed throughout countries and regions, with diverse host types (Madison-Antenucci et al., 2020). Ticks can be a tremendous hazard to human

health, livestock production and wildlife (Tian et al., 2025), and the world's economic losses are more than $18 billion a year (Calvano et al., 2019). Due to the excellent environmental compatibility, the distribution range of ticks has expanded (Moustafa et al., 2025), and numerous novel tick-borne viruses capable of infecting humans have been identified (Sahara et al., 2019; Yuan et al., 2025; Zhang et al., 2019; Zhang et al., 2024; Zhang et al., 2025). Against the background of increasingly severe global warming, heat stress tolerance is crucial for ecological adaptability and population expansion capacity of ticks. *H. longicornis* has successfully invaded many regions (Moustafa et al., 2025; Tian et al., 2025), and therefore the research on the mechanism of heat stress tolerance of *H. longicornis* requires urgent investigation.

Global climate change includes a substantial increase in the frequency and intensity of extreme high temperatures which effects arthropods lifespan and fertility, also pose a threat to the survival of arthropod individuals and populations (Guillén et al., 2022; Ma et al., 2021; Sánchez-Guillén et al., 2016). Arthropods, as ectothermic animals whose life activities are restricted by environmental conditions, are highly sensitive to alterations in environmental temperature. The heat stress responses of arthropods mainly includes altering the lipid utilization, synthesizing osmotic protective metabolites such as trehalose and sorbitol, and inducing the genes expression of heat shock proteins (HSPs) and antioxidant defense (Li et al., 2022). Exposed to heat stress, the neuroendocrine system triggers rapid adipokinetic hormone (AKH) secretion and AKH release into the hemolymph, and the mobilization of glycogen and triacylglycerol in the fat body via the AKH/adipokinetic hormone receptor (AKHR) axis drives sugar or lipid utilization (Bobrovskikh & Gruntenko, 2023). In addition, heat stress also activates amines and hormone, like dopamine, octopamine, and juvenile hormone (JH), that interact with AKH in response heat stress and repair heat-damaged (Bobrovskikh & Gruntenko, 2023). The increase of fructose

availability triggers activity of pentose phosphate pathway, and provides the substrate and coenzyme for polyols synthesis (Salvucci et al., 1999). And the accumulation of sugars, polyols, and amino acids can protect cell structure stability and response to heat stress injury (Li et al., 2023). HSPs as molecular chaperones, play a vital role in protecting organisms and induced by multiple abiotic stresses such as heat, cold, anoxia, and insecticides (Fang et al., 2021; King & MacRae, 2015). Many genes within the HSP family are proven to have the function of responding to heat stress in various species, containing HSP70, HSP26 and HSP83 (Amstrup et al., 2024; Benoit et al., 2011; Sivan et al., 2017). Exposure to heat stress resulted in the increase in the metabolic rate and the reactive oxygen species (ROS) of arthropods (Colinet et al., 2015), which was relieved by antioxidants intake as Vitamin C or dehydroascorbic acid (DHA) (Hwang et al., 2025). And heat stress also up-regulated the expression of superoxide dismutase (SOD), catalase (CAT), and peroxidase (POD) activities to avoid the damage to cells caused by ROS accumulation to maintain the physiological functions (Khurshid et al., 2021; Li et al., 2022).

In addition, the microbiota also plays a positive role in the host's ecological adaptability and stress tolerance. It has been confirmed in various arthropods that symbionts can assist the host in heat stress resistance. *Serratia symbiotica*, as a common facultative symbionts in *Acyrthosiphon pisum*, relieve the detrimental effects of heat stress and improve host fitness (Oliver et al., 2010; Zhou et al., 2021). Compared with the *Rickettsia*-free population, the *Rickettsia*-containing whitefly *Bemisia tabaci* B biotype significantly increases tolerance to heat stress even reaching 40°C, and the tolerance is not dependent on HSP gene expression (Brumin et al., 2011). In reproduction stage, symbionts also play a important role in heat stress tolerance. After a short heat stress during the juvenile stage, compared with the aphids bearing symbionts with short allele, the aphids bearing symbionts possessed a greater number of progeny and symbiont

content (Dunbar et al., 2007). Under the heat stress, *Rickettsia*-infected whiteflies produced more progeny, and had a higher female sex ratio (Himler et al., 2011).

H. longicornis is mainly distributed in Asia, and has strong ecological adaptability. As important vectors, *H. longicornis* transmits various pathogens, like *Coxiella burnetii*, *Borrelia burgdorferi*, and *Babesia ovata* (Mezouar et al., 2025; Price et al., 2021; Yu et al., 2011). Since *H. longicornis* was first recorded in the United States in 2017, it has successfully invaded more regions in rencent years (Moustafa et al., 2025; Tian et al., 2025). *Coxiella*-like endosymbiotic was a nutritional symbionts are crucial for the survival of *H. longicornis* that specifically distributed in the ovaries and malpighian tubules of female ticks, and could 100% vertical transmission to the posterity (Liu et al., 2013). In reproduction stage, the CLE-Hl also could stimulate female ticks to engorgement (Zhong et al., 2021), provide the nutritional support at the end of ovulate stage by recycling metabolites from malpighian tubules (Cibichakravarthy et al., 2022), and synthesis vitamin B and amino acids (Duron et al., 2018; Duron & Gottlieb, 2020; Gottlieb et al., 2015; Smith et al., 2015). Using antibiotics to inhibit CLE-Hl can make a negative impact on *H. longicornis* reproduction (Zhang et al., 2017; Zhong, 2012). The role of ticks endosymbiotic under stress-conditions wasn't expounded. Through field investigations, diel activity of *H. longicornis* revealed that the major activity temperature was between 25°C and 40°C from 10:00 to 14:00, however, the activity of *H. longicornis* was also detected from 5.7°C to 42.1°C (Noh et al., 2024). In order to understand the ecological adaptability and population expansion capacity of *H. longicornis*, the research on the mechanism of heat stress tolerance of requires urgent investigation.

In the present study, we found that exposing the engorged female ticks to transient extreme heat did not affect the survival, and only limitedly impacted the reproduction. Furthermore, by the

111 microbiome, metabolome and transcriptome analyses of ovary, it was confirmed that CLE-Hl
112 and the *HSP68* gene play an important role in restoring the reproductive capacity of the engorged
113 female ticks after transient extreme heat treatment. Overall, these results provide resource for
114 understanding the heat stress tolerance mechanism and ecological adaptability of *H. longicornis*.

115 **MATERIALS AND METHODS**

116 **Ticks rearing**

117 *H. longicornis* was obtained from the Xiaowutai National Nature Reserve, Hebei Province,
118 China (E114°47′–115°28′, N39°50′–40°6′). During the non-parasitic stage, ticks were cultured
119 in an environmental chamber (temperature=26±1°C, relative humidity=75±5%, light:
120 darkness=16h:8h). At the parasitic stage, ticks were allowed to feed on the ears of New Zealand
121 white rabbits.

122 **Transient extreme heat treatment and sample collection**

123 Collecting the engorged female *H. longicornis*, the ticks were excluded that oversize (over
124 0.2500 g) or undersize (lower than 0.1500 g), and then the ticks were randomly divided into two
125 groups. The high-temperature group was directly placed in 42°C (relative humidity=75±5%) for
126 30 min, and cultured in the environmental chamber (temperature=26±1°C, relative
127 humidity=75±5%). The untreatment group was cultured in the environmental chamber directly
128 (temperature=26±1°C, relative humidity=75±5%).

129 The accordingly groups of ticks were dissected and moved into 1×PBS (Solarbio, China) to
130 obtain the ovaries. After washing by 1×PBS (Solarbio, China) three times, the ovaries were
131 labelled to follow-up studies.

Bright-field imaging

The different treatment groups of ticks, ovaries, eggs and offspring generation larvae were observed with a microscope (Carl Zeiss Microscope GmbH, Germany).

Transmission electron microscope (TEM) imaging

The ovaries of *H. longicornis* were dissected and immediately fixed in 4% glutaraldehyde for 4h at 4°C. The sample was moved to a 1/15 mol/L phosphate buffer solution for 12h, and then 1% osmium tetroxide was added for 2h at 4°C. After washing in 1/15 mol/L phosphate buffer solution, the sample was dehydrated using increasing concentrations of acetone (30%, 50%, 70%, 80%, 90%, and 95%) for 25 min each step, followed by three washes with 100% anhydrous acetone at 4°C, 25 min each. Subsequently, the samples were infiltrated with increasing concentrations of Agar 100 resin in propylene oxide: 50% for 3h, 75% for 12h, and 100% for 12h at 37°C. The samples were dried in an incubator at 37°C for 12h and at 60°C for 48h. The samples were sectioned with a diamond knife and collected onto thin copper bar grids (100 mesh). The sections on the grids were stained with uranyl acetate for 8 min and with lead citrate for 5 min and then viewed with a model H-7650 transmission electron microscope (Hitachi, Japan).

Reproductive ability assay

To estimate reproductive ability of accordingly groups, the reproductive efficiency index (REI) and hatchability were performed. For one single female, the weight of engorgement ticks and all eggs were measured by electronic balance, and the REI was calculated.

$$\mathrm{REI} = \frac{\text{the weight of all eggs}}{\text{the weight of engorgement ticks}} \quad (1)$$

153 For all the female in group, all eggs were completely mixed and labelled. After 30 days of
154 cultivation, the hatchability was calculated.

155 $$\text{Hatchability} = \frac{\text{the amounts of offspring generation larvae}}{\text{the amounts of eggs}} \quad (2)$$

156 ***16S ribosomal RNA* gene high-throughput sequencing**

157 The ovary samples of the untreatment group and the high-temperature group were collected and
158 separately washed by 70% ethanol, sterile and nuclease-free dH_2O three times to avoid
159 environmental contamination. DNA extraction was performed using a QIAamp Fast DNA Stool
160 Mini Kit (Qiagen, USA). The concentration and quality of DNA were measured using Nanodrop
161 2000 (Thermo Scientific, USA) and 1% gel electrophoresis detection, respectively.

162 Barcode-indexed primers (338F: 5′–ACTCCTACGGGAGGCAGCAG–3′; 806R: 5′–
163 GGACTACHVGGGTWTCTAAT–3′) were used to amplify the V3–V4 region of the bacterial
164 *16S ribosomal RNA* (*rRNA*) gene by TransStart Fastpfu DNA Polymerase (TransGen, China).
165 And sterile ddH_2O was used as negative control for PCR. The amplicons were purified by
166 AxyPrep DNA Gel Extraction Kit (Axygen Biosciences, USA), and then were quantified using
167 QuantiFluor-ST (Promega, USA). The purified productions were pooled in equimolar
168 concentrations. The paired-end sequencing was performed on the Illumina MiSeq PE300
169 platform (Majorbio Bio-pharm Technology, China). The further analyses, including merging and
170 filtering the MiSeq sequence data by the Trimmomatic software (Bolger et al., 2014), aligning to
171 Silva database (Pruesse et al., 2007), screening for chimeras by Uchime algorithm (Edgar et al.,
172 2011), grouping (over 97% similarity) into operational taxonomic units (OTUs) by OptiClust
173 clustering algorithm (Westcott & Schloss, 2017), processing OTU table in Qiime (MACQIIME

v.1.9.0) (Caporaso et al., 2010), taxonomically assigning by RDP Classifier v.2.2.0 (Wang et al., 2007), obtaining the Greengenes *16S rRNA* database v.13.5.0 (with 70% confidence) (McDonald et al., 2012), and summarizing OTU in all levels, were performed by the platform of Majorbio (https://www.majorbio.com/tools). The α-diversity indices, Shannon index, was calculated to measure bacterial community richness and diversity between the high-temperature group and untreatment group by Mothur v.1.30.1 (Schloss et al., 2009). Beta diversity was calculated by weighted and unweighted UniFrac analysis (Lozupone & Knight, 2005) to plot the differences by principal coordinate analysis (PCoA). The co-occurrence network analysis was performed by the iNAP2 (https://inap.denglab.org.cn/) (Peng et al., 2024).

DNA-fluorescence in situ hybridization (FISH)

The ovaries was dissected and immersed in 4% paraformaldehyde for 24h at –4°C. The protocol followed the method of Buysse *et al*. (2019). Samples were preincubated with 200 μL of hybridization buffer [20×SSC Buffer (Solarbio, China)/50×Denhardt's solution (Solarbio, China), v:v = 1:1] for 15 min and then moved to 200 μL HB containing 1 μL of probe and incubated for 16h at 46°C. The DNA-FISH probe for CLE-HL was 5'–CY3–GACTTCCCACATCGTTT–3', as used by Wang *et al*. (2018). Samples were washed with 200 μL of pre-warmed washing buffer [20 mmol/L TrisHCl pH 8.0 (Solarbio, China)/80 mmol/L NaCl/50 mmol/L EDTA (Solarbio, China)/0.01% SDS (Solarbio, China)] for 30 min at 48°C and then washed with 1 mL of PBS (Solarbio, China) for 15 min. The samples were incubated with DAPI (Thermo Fisher Scientific, USA) to label the nuclear DNA. Fluorescent signals were observed with a fluorescence microscope (Carl Zeiss Microscope GmbH, Germany).

Vitamin B rescue in transient extreme heat treatment female ticks

196 To verify the lack of the eggs' CLE-Hl leading the low hatching rate of the high-temperature
197 group, ten kinds of vitamin B, multivitamin, and DEPC-H_2O were injected to females after 24h
198 of the transient extreme heat treatment, respectively. The working concentrations of ten kinds of
199 vitamin B and multivitamin were listed in Supplementary Table S1, and the microinjections were
200 performed with 1 μL of vitamin B or DEPC-H_2O per engorged female tick.

201 **Transcriptome analysis**

202 The ovary samples of the untreatment group and the high-temperature group were collected, with
203 three replicates in each groups. The samples were sent to Majorbio Bio-Pharm Technology Co.
204 Ltd. (China) for transcriptomic sequencing. Sequencing libraries were constructed using the
205 Hieff NGS Ultima Dual-mode messenger RNA (mRNA) Library Prep Kit (Yeasen, China) and
206 sequenced on the Illumina NovaSeq platform. The bioinformatics analyses, including the quality
207 control, sequence alignment, transcript prediction, gene annotation, expression level calculation,
208 differential transcripts expression analysis (*P*-value<0.05 and fold change>1.2 or <0.83), Gene
209 Ontology (GO) enrichment analysis and Kyoto Encyclopedia of Genes and Genomes (KEGG)
210 enrichment analysis, were performed by the platform of Majorbio
211 (https://www.majorbio.com/tools). The reference genome of *H. longicornis*
212 (GCA_013339765.2_BIME_HaeL_1.3) was downloaded from the National Center for
213 Biotechnology Information database (https://www.ncbi.nlm.nih.gov/datasets/genome/).

214 **Metabonomics analysis**

215 The 100 mg ovary sample of the untreatment group and the high-temperature group with six
216 replicates in each groups were ground and added 800 μL extraction solution (methanol: water =
217 4:1 (v:v) with four internal standards (0.02 mg/mL L-2-chlorophenylalanine, etc.). Samples were

kept at –20°C for 30 min, and then centrifuged at 13000×*g* for 15 min (4°C). The supernatants were used for Liquid Chromatography-Tandem Mass Spectrometry (LC-MS/MS) analysis. For quality control process, the quality control (QC) sample was mixed by the equal volumes of all samples and tested in the same manner as the analytic samples. The LC-MS/MS analysis of 12 samples were managed on a UHPLC-Orbitrap Exploris 480 system with the ACQUITY HSS T3 column (100 mm×2.1 mm i.d., 1.8 μm; Waters, USA) at Majorbio Bio-Pharm Technology Co. Ltd. (China). For the chromatographic, the condition setting as solvent A (0.1% formic acid in water:acetonitrile=2:98, v/v) and solvent B (0.1% formic acid in acetonitrile) in the mobile phases with the flow rate was 0.40 mL/min (the column temperature=40℃). The UPLC system was jointed to the UHPLC-Orbitrap Exploris 480 system mass spectrometer with the electrospray ionization (ESI) source operating in positive mode and negative mode. For the mass spectrometer, the conditions setting as that sheath gas flow rate was 40 arb, aux gas flow rate was 10 arb, source temperature was 400℃, ion-spray voltage floating (ISVF) was 3500V for the positive mode and –2800V for the negative mode, and normalized collision energy was 4. And the data acquisition was enforced the Data Dependent Acquisition (DDA) mode with a mass range of 70-1050 m/z.

The raw data was performed by Progenesis QI (Waters Corporation, USA) software and was exported in CSV format which including sample information, metabolite name and mass spectral response intensity. Internal standard peaks and false positive peaks were removed, deredundant and peak pooled. The metabolites were identified by searching database including the HMDB (http://www.hmdb.ca/), Metlin (https://metlin.scripps.edu/) and the self-compiled Majorbio Database (MJDB) of Majorbio Biotechnology Co., Ltd. (Shanghai, China). For data matrix pre-processing, over 80% of the metabolic features detected in any set of samples were reserved. The

response intensities of the sample mass spectrometry peaks were normalized using the sum normalization method. The variables of QC with relative standard deviation (RSD)>30% were excluded, and $\log_{10}$ logarithmicized. The further analyses, including the perform variance analysis, principal component analysis (PCA) and orthogonal least partial squares discriminant analysis (OPLS-DA) by R package "ropls" (Version 1.6.2), different metabolites analysis [Variable importance in the projeciton (VIP)>1, P<0.05], and KEGG enrichment analysis by the Python packages "scipy.stats" (https://docs.scipy.org/doc/scipy/), were performed by the platform of Majorbio (https://www.majorbio.com/tools).

RNA interference

The double-stranded RNA (dsRNA) was synthesized using a MEGAscript RNAi Kit (Thermo Fisher Scientific, USA) to verify the function of three candidate genes. Based on the cDNA sequences, primers with a T7 promoter sequence were designed; these are listed in Supplementary Table S2. The *green fluorescent protein* (*GFP*) (KX247384.1) was used as the exogenous control (Gong et al., 2009). The dsRNA was dissolved in RNase-free dH_2O (Invitrogen, USA), and microinjections were performed with 20,000 ng of dsRNA per engorged female tick. After 24h, 48h and 72h post-injection, five ovaries from different treatment groups were dissected as a single sample (three biological replicates for each group).

RNA extraction

Total RNA of tick ovaries was purified using the TRIzol reagent (Invitrogen, USA) following the manufacturer's instructions. cDNA was synthesized using 400–600 ng RNA by the Verso cDNA Synthesis Kit (Thermo Fisher Scientific, USA). The concentration and quality of RNA and cDNA were measured using Nanodrop 2000 (Thermo Scientific, USA) and 1% gel electrophoresis detection, respectively.

264 **DNA extraction**

265 For detecting the relative numbers of CLE-Hl, the total DNA of tick ovaries was purified using
266 an *EasyPure*®Genomic DNA Kit (TransGen Biotech, China). The concentration and quality of
267 DNA were measured using Nanodrop 2000 (Thermo Scientific, USA) and 1% gel
268 electrophoresis detection.

269 **Quantitative real-time PCR (qPCR)**

270 To measure gene interference efficiency and relative amounts of CLE-Hl by qPCR, a
271 MagicSYBR Mixture (CwBiotech, China) was employed following the manufacturer's
272 instructions. The cDNA and total DNA of treatment groups were quantified using a Roche
273 LightCycler 480 (Roche, USA). The reactions for each sample and *GFP* were run in duplicate.
274 Gene interference efficiency was determined by relative quantification normalized to *actin*
275 (EU019716.1). Relative amounts of CLE-Hl were determined by absolute quantification. The
276 *pEASY*®-T1 Simple Cloning Kit (TransGen Biotech, China) and an *EasyPure*® Plasmid MiniPrep
277 Kit (TransGen Biotech, China) were used to construct plasmids containing the target genes, ropb
278 of CLE-Hl and actin of *H. longicornis*, and to draw the standard curve. The primers are listed in
279 Supplementary Table S2.

280 **Statistics**

281 The Student's *t*-test was used to compare statistical significance between two groups. One-way
282 ANOVA test was used to compare statistical significance among different treatment groups, and
283 Tukey's multiple comparison was used for post hoc analysis. $P<0.05$ was considered statistically
284 significant. Data analysis was carried out using Graph Prism version 8.0.2 for Windows
285 (GraphPad Software, USA).

RESULTS

Effect of transient extreme heat on reproduction

The transient extreme heat treatment would not have any impact on the survival ability of female ticks, but the ovarian development was seriously delayed. In untreatment group, the bright-field images of ovary revealed that the oocytes outside the ovarian longitudinal groove turning light-yellow from the 1 day post treatment (dpt), and the mature oocytes presenting in ovariole from the 3 dpt (Figure 1A). By contrast, in high-temperature group, the ovarian bright-field images displayed obvious inhibition of development that the oocytes keeping opalescent at the 1 and 2 dpt, the vitellogenin accumulating from the 3 dpt, and the mature oocytes presenting in ovariole from the 5 dpt (Figure 1A). Surprisingly, the maturation of oocytes are similarity from the 10 dpt at two groups (Figure 1A). To describe the characteristic of egg-laying in two groups, the daily productive efficiency of females were quantified. In untreatment group, the laying of eggs begins at the 4 dpt and peaks at the 6 dpt, but in high-temperature group the laying of eggs begins at the 5 dpt and peaks at the 8 dpt (Figure 1B). The TEM was performed to explore more details about the inhibition of ovarian development after the transient extreme heat treatment. Compared with untreatment group, at the 1 dpt the oocytes in high-temperature group contains large numbers of grey granules, and the mitochondria with intumescent form and quantity increasing (Figure 1C). At the 3 dpt the oocytes in high-temperature group shows further abnormalities that the vitellogenin granules with the rough surfaces (Figure 1C). Comparison of ovarian morphology at the peak of ovulation, in untreatment group the eggshell is structurally complete and thick, and containing granular protein, but in high-temperature group the eggshell is thin and uneven (Figure 1C).

The reproductive ability is slight decrease after the transient extreme heat treatment, but have not significant difference. The REI decrease from 0.4740±0.01476 in untreatment group to 0.4518±0.02090 in high-temperature group (P=0.3730) (Figure 1D), and the weight of egg-laying decrease from 0.1011± 0.00383 in untreatment group to 0.0911±0.00597 in high-temperature group (P=0.1418) (Figure 1E). Although the transient extreme heat treatment does not affect the reproductive ability of female ticks, the eggs of high-temperature group ticks show a significant proportion of withered and paler color. Furthermore, the hatching rates of eggs were calculated, in the high-temperature group the hatching rate is significant reduction to 62.14±0.836% than the 89.38±0.462% in untreatment group (Figure 1F). The hatching process of eggs were recorded, the high-temperature group eggs retards than untreatment group, and some of them appearance of arrested-developing eggs (Figure 1G). In two groups, the phenotype of offspring generation larvae has a little difference in the body color. The larvae in high-temperature group are pale yellow, which due to the abnormal of midgut (Figure 1H). In summary, the transient extreme heat partly impacts the reproduction of ticks, but the influences gradually be repaired by the unknown mechanisms.

16S rRNA sequencing

To explore the impact of temperature variation to microbiota of ovary, at the 3 dpt, the microbiota in two groups ovary was detected by *16S rRNA* sequencing. The diversity of six samples in two groups was analyzed. After removing the low-quality reads, a total of 348 212 optimized sequences were obtained which totally 149 205 445 bp, and the average length of reads was 428 bp. Perform the OTUs clustering analysis on non-redundant sequences based on a 97% similarity criterion, the details were listed in Supplementary Table S3. The bacterial microbiota was assigned to 11 phyla, 20 classes, 41 orders, 61 families, 93 genera, and 103

331 species. The venn diagram showed the amounts of unique and shared OTUs in phylum, class,
332 order, family, genus, and species levels, respectively (Figure 2A; Supplementary Table S4). By
333 comparison, after transient extreme heat treatment the bacterial richness was slight increase. The
334 proportions of the top 10 dominant bacteria in phylum, family, and genus levels are shown in
335 Figure 2B, respectively. The main change of proportions of bacterial microbiota was brought by
336 the CLE-Hl increase. Bacterial community diversity (Shannon index) showed no significant
337 difference (P=0.149) between the two groups at the OTU level (Figure 2C). Principal Co-
338 ordinates Analysis (PCoA) based on Bray-Curtis distance showed a trend of separation between
339 the two groups, but PERMANOVA revealed no significant difference (P=0.098) (Figure 2D). To
340 further analyze the impact on the microbial community, the co-occurrence network analysis was
341 performed to understand the potential symbiotic relationships of the ovarian microbiota in
342 transient extreme heat stress (Figure 2E; Table 1). While in the network of untreatment group, 71
343 OTUs were enriched, with an average weighted degree of 22.645, a diameter of 2, and an
344 average path length of 1.245161 (Figure 2E; Table 1). But, in the network of the high-
345 temperature group, 31 OTUs were enriched, with an average weighted degree of 18.845, a
346 diameter of 3, and an average path length of 1.74004 (Figure 2E; Table 1). It is revealed that the
347 ovarian microbiota subjected to a significant impact that the reduction of connectivity and the
348 weakned of potential interaction after the ransient extreme heat treatment. Basing the closeness
349 centrality to screen the hub-nodes in co-occurrence network, the top 10 nodes that appear most
350 frequently on the shortest connection path of two groups were listed in Table 2. The results
351 reflected that the hub-nodes of untreatment group were disappeared after the transient extreme
352 heat treatment, and the new hub-nodes of high-temperature group were formed by the microbiota
353 at periphery of network except the OTU63 (*Methyloversatilis*) (Table 2). In contrast, the mutual

OTUs in the two groups confirmed that the six OTUs (OUT60, OTU28, OTU74, OTU38, OTU29 and OTU31) in the Module 4 of untreatment group were reformed the new hub of high-temperature group (Figure 2E; Table 2). Among them, the hub-nodes, OUT60 (*Pseudomonas brenneri*), OTU28 (uncultured *Caulobacteraceae*) and OTU74 (*Bradyrhizobium japonicum*), may provide support for the formation of multi-species biofilms. In addition, the *Methyloversatilis*, which specificity in the high-temperature group, have played a role in promoting the ovarian development in *Portunus trituberculatus* (Wei et al., 2020). Although in two co-occurrence networks the OTU44 (CLE-Hl) are located at the periphery, its contents hold an absolute dominance within the microbiota and increases after the transient extreme heat treatment. As the most important endosymbiotic bacteria during reproduction of *H. longicornis*, the CLE-Hl has a relatively distant relationship with other bacterial of microbiota for community, but has a close relationship with the host. Although the contents of CLE-Hl is high, its dependence on other bacterial of network is relatively low. The details of CLE-Hl potential functions were further investigation.

Effect of transient extreme heat on ovarian CLE-Hl

The relative amounts of ovarian CLE-Hl in two groups were revealed from the 1 dpt to 8 dpt, separately (Figure 3A; Supplementary Figure S1). After transient extreme heat treatment, the relative amounts of ovarian CLE-Hl were increase, especially in the 1 dpt, from the 10.97±0.52 in the untreatment group increasing to 98.71±3.33 in the high-temperature group (Figure 3A), which implied the CLE-Hl may be involved in assisting the host in heat stress resistance. The distributions of CLE-Hl at the 1 to 8 dpt were exposed by the DNA-FISH assay (Figure 3B). By contrast, in high-temperature group, the CLE-Hl distribution range has expanded and it is widely present in oocytes at the 1 and 2 dpt (Figure 3B^{a-d}). At the 4 dpt, the difference in CLE-Hl

distribution between two groups was concentrated in the oocytes inside the ovarian longitudinal groove which have a high density in the high-temperature group (Figure 3B$^{g, h}$). From the 5 dpt, the difference focuses on the oocytes outside the ovarian longitudinal groove which having a large volume with a significant accumulation of vitellogenin (Figure 3B$^{i\text{-}p, i'\text{-}p'}$). In the untreatment group, the CLE-Hl aggregated on one side of oocytes and showed a layered distribution till the 8 dpt (Figure 3B$^{j', l', n', p'}$). But in the high-temperature group, the layered distribution of CLE-Hl showed incomplete that contrary to the high relative amounts within the ovaries, and the phenomenon was gradually intensifying (Figure 3B$^{i', k', m', o'}$). To confirm this phenomenon, the relative amounts of eggs' and offspring generation larval CLE-Hl were revealed. Surprisingly, although the relative amounts of CLE-Hl in the high-temperature group ovaries increased, the relative amounts of CLE-Hl within the eggs' and offspring generation larval significantly decreased (eggs: untreatment group=7.539±0.1198, high-temperature group=4.250±1.3047; larval: untreatment group=7.003±0.0995, high-temperature group=4.094±0.0340) (Figure 3C, D), which implied the additional CLE-Hl is mainly involved in the host's response to heat stress.

Effect of Vitamin B rescue on reproduction after transient extreme heat treatment

During reproduction, the CLE-Hl providing the nutritional support at the end of the ovulate stage by synthesizing vitamin B. At the 3 days post injection (dpi), the ovaries of the 12 groups were obtained and collected images in the bright-field and fluorescence-field microscope. Compared with the DEPC-H_2O group, ovaries of all other groups showed development restoration in the bright-field, especially in the vitamin B2, vitamin B6, vitamin B7, vitamin B9 and multivitamin groups (Figure 4A$^{a–l}$). In the fluorescence-field, the CLE-Hl distribution in the vitamin B2, vitamin B6, vitamin B7, inositol and multivitamin groups were expanded and content increase

than the DEPC-H_2O groups (Figure 4A[a'–l']). Furthermore, the eggs of vitamin B rescue groups displayed obvious color differences. In the vitamin B1, vitamin B2, vitamin B5, vitamin B7 and vitamin B12 groups the color of eggs becomes lighter (Figure 4B[c', d', f', h', j']), in the vitamin B3, vitamin B6 and inositol groups the color of eggs becomes darker and turns back to amber (Figure 4B[e', g', l']), and in the vitamin B9 and choline chloride groups the color of eggs turns to a grayish-brown (Figure 4B[i', k']). The daily productive efficiency in vitamin B rescue groups revealed that the Vitamin B rescue It is failed to recover the time of egg-laying, but in vitamin B2, vitamin B5, vitamin B7 and multivitamin groups it can help to promote the egg-laying peak (Figure 4C). The REI of the vitamin B rescue groups verified the vitamin B1, vitamin B3, vitamin B5, vitamin B6, vitamin B7, vitamin B9, choline chloride and multivitamin rescue could increase the fertility of transient extreme heat treatment females (Figure 4D). Except the vitamin B7 rescue group, the hatching rates of eggs in other groups are significant increase, especially in the multivitamin group the hatching rate reaches to 97.20±0.318% (P<0.0001) which exceeding the untreatment group (89.38±0.462%) in Figure 1F, and the vitamin B2 (88.96±0.292%, P<0.0001) and inositol (89.50±0.442%, P<0.0001) rescue groups are also close to those of the untreatment group (Figure 4E). The hatching rates of eggs in Vitamin B rescue groups confirmed the hypothesis that the reduction of eggs' CLE-Hl content due to additional consumption of ovarian CLE-Hl in heat stress, which causing the decreased vitamin B supply, and led to the low egg hatching rate.

Metabonomics analysis

The ovarian metabonomics of the high-temperature and untreatment group at the 3 dpt were detected to explore the effects of the transient extreme heat treatment. The metabolites were analysed, identified and annotated through liquid chromatography. Totally, it was obtained 548 metabolites in positive model and 257 metabolites in negative model. The component of

metabolites was slightly alterated that only contant two specifically metabolites in the untreatment group at positive and negative model, separately (Supplementary Figure S2). The metabolites annotated in the KEGG database were classified, and the results are presented in Supplementary Figure S3. The differential metabolites (DMs) (VIP>1，*P*-value<0.05)were calculated, it is shown that 34 metabolites had significantly increased, and 49 metabolites had significantly decreased (Supplementary Figure S4). The top 30 marker metabolites were screened from DMs (Supplementary Figure S5). Except the short peptides, the marker metabolites including some prominent secondary metabolites of pivotal enzymes in metabolism alteration, as queuine, osmaronin, dynorphin B (6-9), 4-hydroxynonenal and paxilline (Supplementary Figure S5). The DMs were enriched in KEGG database, and the top 20 pathways were shown in Figure 5A which most of the pathways were amino acid metabolism-related pathways. Except that, the "pentose phosphate pathway (map00030)" and "pantothenate and CoA biosynthesis (map00770)" were enriched, which indicating the energy utilization mode was change after the transient extreme heat treatment. The enrichment of "linoleic acid metabolism (map00591)", "alpha-linolenic acid metabolism(map00592)", "glycerophospholipid metabolism (map00564)" pathways implied the temperature changes leading to alteration in lipids utilization. It is indicated the transient extreme heat treatment caused utilization changes of sugar and lipid. The "drug metabolism-other enzymes (map00983)" pathway indicated that the heat stress resultes in the oxidative damage repair. The enrichment of "neuroactive ligand-receptor interaction (map04080)" and "ABC transporter (map02010)" pathways suggested the heat stress triggered the transport of a wide variety of substrates such as hormones, sterols, lipids and ions to protect cell structure stability and response to heat stress injury.

Transcriptome analysis

446 The ovarian transcriptome of the high-temperature and untreatment group at the 3 dpt were
447 sequenced to explore the effects of the transient extreme heat treatment. Totally 55.28 Gb of
448 Clean Data was obtained, and each sample reached more than 7.39 Gb (Supplementary Table
449 S5). The percentage of Q30 base was more than 96.31%, and the average sequencing error rate
450 was 0.0117% (Supplementary Table S5). The GC content was between 51.87% and 52.27%, and
451 the values of samples in two groups were similar (Supplementary Table S5). The Clean Reads
452 were aligned with the genome of *H. longicornis*, and the alignment rate ranged from 79.56% to
453 79.85% (All of the alignment rates exceeded 70%), indicating that the sequence alignment
454 results could be used for subsequent analysis (Supplementary Table S6). The quality evaluations
455 were performed (Supplementary Figure S6; Supplementary Figure S7), the transcripts were
456 assembled and annotated (Supplementary Figure S8; Supplementary Figure S9), and distribution
457 of transcription expression in six samples was displayed (Supplementary Figure S10). Analyzed
458 the amounts of unique and shared genes between the two groups, it is showed that the 260 genes
459 specifically expressed in the high-temperature group, the 239 genes specifically expressed in the
460 untreatment group, and the 6 875 genes expressed in both groups (Supplementary Figure S11).
461 The differentially expressed genes (DEGs) were revealed (Supplementary Figure S12;
462 Supplementary Figure S13), and the directed acyclic graph based on the GO database enrichment
463 revealed that the enriched GO terms mainly perform three types of functions as the metabolic
464 process regulation triggering by proteolysis (The aqua background), the molecular function
465 regulating by serine-type endopeptidase (The golden-amber background), and the cellular
466 response to superoxide radical stress (The light-pink background) (Supplementary Figure S14;
467 Supplementary Figure S15). The DEGs were enriched in the KEGG pathways by GSEA to
468 explore more details, the enriched pathways (Supplementary Figure S16). The enriched

pathways in genetic information processing and cellular processes conformed to that the transient extreme heat treatment formed a severe DNA double strand damage but the damage only triggered the cell cycle arrest not cellular senescence or apoptosis. The enriched pathways in organismal systems showed the high-temperature group increased energy and substance demand, and initiated cell survival mechanisms. In addition, the enrichment of the "estrogen signaling pathway (map04915)" and "cholinergic synapse (map04725)" pathways suggested the hormones system and peripheral nervous system in ovary also involved in the recovery after heat stress. The enrichment of pathways in environmental information processing and metabolism categories implied the changes in cell membrane, extracellular structures and intercellular connection structures. Remarkably, the up-regulation of "riboflavin metabolism (map00740)" pathway indicated the accumulation of riboflavin exceeding the requirement. The enriched DEGs in KEGG database were visualization which containing the 78 up-regulated genes and the 46 down-regulated genes (Figure 5B). The function of enriched DEGs could be divided into the lysosome, ubiquitination, immunoreaction, chitin relevant, apoptosis, cell signal, neural signal, cellular community, genetic information processing, metabolism and energy, others and function unknown genes. Cells avoided heat stress damage by genes expression alteration to change the structure of cell membrane and transporter compositions. Based on the function and the expression foldchange, the *HPB48-0018326* (*cytochrome P450 6a9*, *Cyp6a9*) genes for antioxidant defense, *HPB48-0023605* (*heat shock protein 68*, *Hsp68*) genes for heat shock response, and the *HPB48-0016741* (*chloride channel accessory 2*, *CLCA2*) genes for DNA damage repair were screened as candidate genes to verify the role in the process of repairing heat stress damage.

Roles of candidate genes in transient extreme heat on reproduction

The three candidate genes were performed for RNA interference, and the interference efficiency of three genes were detected at 24h, 48h and 72h post-injection (hpi) in ovary (Figure 5C). The interference efficiencies of the *CLCA2* genes were 64.6% at 24 hpi and 63.6% at 48 hpi, separately. In the *Hsp68* genes interference group, the interference efficiencies were 35.2% at 24 hpi and 52.0% at 48 hpi. And the interference efficiencies of the *Cyp6a9* group were 30.1% at 24 hpi, and 74.2% at 48 hpi. The bright-field images of ovary displayed the effect of candidate genes interference to the fecundity after the transient extreme heat treatment (Figure 5D). At 24 hpi, the ovaries of *Hsp68*, *CLCA2* and *Cyp6a9* groups were significantly developmental inhibition than the *GFP* group. At 48 and 72 hpi, the ovaries of *Hsp68* and *CLCA2* groups were maintained inhibition, but the *Cyp6a9* group similar with the *GFP* group. Compared with the *GFP* group (0.09089±0.007771), the weight of egg-laying decrease in three RNA interference group. Although there was no significant difference in *CLCA2* group (0.06557±0.008337, P=0.0951), both *Hsp68* (0.04289±0.005099, P=0.0003) and *Cyp6a9* (0.05942±0.009909, P=0.0230) groups showed a significant decrease (Figure 5E). The REI decrease from 0.4054±0.02742 in *GFP* group to the 0.2197±0.02745 (P=0.0018) in *Hsp68* group, the 0.3230±0.03371 (P=0.2870) in *CLCA2* group, and the 0.2940±0.04663 (P=0.0884) in *Cyp6a9* group (Figure 5F). In summary, the above results indicate that the specific up-regulation of the three candidate genes plays a pivotal role in the recovery of reproductive capacity after transient extreme heat treatment, especially the *Hsp68* gene plays the most crucial role.

DISCUSSION

As a blood sucking arthropod, *H. longicornis* is mainly distributed in Asia with an expanding distribution range, and has excellent ecological adaptability. The field investigations revealed that *H. longicornis* have the capacity of tolerating environment temperature of 5.7°C to 42.1°C

(Noh et al., 2024). In order to understand the heat stress tolerance and ecological adaptability of *H. longicornis*, we exposed the engorged female ticks to transient extreme heat (42°C for 30 min), and found that the heat stress did not affect the survival of engorged females, and had only limited effects on reproduction. Based on the microbiome, metabolome and transcriptome analyses, it was confirmed that *H. longicornis* has a series of complex heat stress repair mechanisms, and the endosymbionts CLE-Hl and the *HSP68* gene play an important role in heat stress tolerance of *H. longicornis*. In summary, this study uncovers details for understanding the heat stress tolerance mechanism and ecological adaptability of *H. longicornis*.

The engorged female ticks have excellent heat tolerance such that transient extreme heat treatment would not have any impact on their survival, and partly impacts reproduction as the ovarian development was delayed and the hatching rates was reduced. However, the weight of egg-laying and REI slightly decrease under the transient extreme heat treatment (Figure 1D, E). The bright-field and TEM images confirmed that the inhibition of ovarian development in the high-temperature group was caused by the heat damage repair (Figure 1A, C). When exposed to high temperatures for over 5 hours, the F1 generation of *Microplitis manila* was suppressed in longevity and fecundity (Ren et al., 2025). Heat stress significantly reduced the survival and fecundity of *Pteromalus puparum* which parasitizes butterfly (Xiong et al., 2023), and inhibited the development and parasitism of *Coccophagus japonicus* (Sun et al., 2024). Moreover, the *B. tabaci* declines in the hatching rate and female sex ratio after expose to 43°C–45°C for 1 hour (Williams et al., 2003). The results of transient extreme heat treated females reflect that *H. longicornis* possess excellently heat stress tolerance and extremely ecological adaptability.

The ovarian microbiota analysis revealed that after transient extreme heat treatment the co-occurrence network forming a new hub which could survive at high temperatures (Figure 2E;

Table 2). The CLE-H1 was located at the edge of the network in both of two groups and interacted with other bacteria less. However, in the high-temperature group the CLE-H1 increased in content which indicated that it might play a role in heat tolerance of *H. longicornis* (Figure 3A). It has been confirmed in various arthropods that symbionts can assist the host in heat stress resistance (Brumin et al., 2011; Oliver et al., 2010; Zhou et al., 2021). Further analysis revealed that the amount of CLE-H1 within the egg decreased to a half (Figure 3C). In consideration of CLE-H1 expressing different protein profile by the location (malpighian tubules or ovary) to cooperate with the organizational functions of host, it is speculated that CLE-H1 increase sharply might have participated in the execution of heat stress damage repair (Figure 6). The Duox-ROS which induced by gut commensal bacteria is vital for maintaining peritrophic matrix (PM) structural, in contrast the PM regulates immune deficiency (Imd) pathway to protect epithelial cells (Bai et al., 2025). The abnormal midgut colour phenotype in offspring larvae was speculated to result from limited vertical transmission of microbiota, leading to insufficient ROS stimulation and thus lack of melanization during PM formation. As a nutritional endosymbiotic, the most important role of CLE-H1 is to provide the required vitamin B to the developmental oocyte. The limited vertical transmission of CLE-H1 caused vitamin B deficient which might result the low hatching rate. After vitamin B rescue to the transient extreme heat treatment females, it was found that in some vitamin B rescue groups, especially in the multivitamin group, the vitamin B2 group and the inositol group, the reduced hatching rate were significantly restored. It was confirmed that the deficiency of vitamin B is the main reason of the hatching rate decrease (Figure 6).

Metabolic and transcriptomic results indicated that the heat stress response of *H. longicornis* was consistent with that of other arthropods, involving alterations in lipid utilization, synthesizing

561 osmotic protective metabolites, and induction of the expression of HSPs genes and antioxidant
562 defense genes. The top 20 enriched pathways of DMs based on KEGG database revealed that the
563 “pentose phosphate pathway (map00030)”, “pantothenate and CoA biosynthesis (map00770)”,
564 and “glycerophospholipid metabolism (map00564)” are associated with alterations in sugar and
565 lipid utilization, while the “ABC transporter (map02010)” is involved in typical osmotic
566 protective metabolites synthesis, with the purpose of protecting cell structure stability (Figure
567 5A; Figure 6). Except the short peptides, the top 30 marker metabolites including some
568 prominent secondary metabolites of pivotal enzymes in metabolism alteration, as queuine,
569 osmaronin, dynorphin B (6-9), 4-hydroxynonenal and paxilline (Supplementary Figure S5).
570 Queuine is a hypermodified nucleobase acting on the first position of the anticodon of tRNAs
571 which is specific for Asn, Asp, His, and Tyr. Queuine is relevant to oxidative stress response,
572 and impairs mitochondrial function and protein folding (Ehrenhofer-Murray, 2025). Osmaronin
573 involved in defense against pathogens and environmental stresses, and is biosynthesized through
574 cytochrome P450 and UDP-glucosyltransferases triggered by the L-leucine (Ehlert et al., 2019).
575 Dynorphin B (6-9) binds to the kappa opioid receptor in the cell nucleus, which triggers a
576 signaling cascade involving nuclear PKC activation to enhance the transcription of key
577 developmental genes (Ventura et al., 2003). As an oxidative stress biomarker, 4-hydroxynonenal
578 (4-HNE) is an endogenous electrophilic lipid peroxidation product and an inhibitor of aldehyde
579 dehydrogenase 2 (ALDH2) whose dehydrogenase activity is related to the metabolism of
580 aldehydes produced under oxidative stress and a pivotal enzyme in insect hormone biosynthesis
581 (Gao et al., 2022). Paxilline belongs to the indole diterpenes class, acts primarily as an inhibitor
582 of calcium-sensitive potassium channels in calcium-activated potassium channels subfamily, and
583 can also inhibit the sarcoplasmic or endoplasmic reticulum Ca^{2+}-ATPase (Ghatta et al., 2006).

584 The directed acyclic graph of DEGs based on GO database revealed that three types of functions
585 as the metabolic process regulation triggering by proteolysis, the molecular function regulating
586 by serine-type endopeptidase, and the cellular response to superoxide radical stress were
587 performed (Supplementary Figure S15), which is consistent with the heat stress response of the
588 metabolic. Screened out the pivotal enriched KEGG pathways by the GSEA, among them, the
589 *Cyp6a9*, *Hsp68* and *CLCA2* genes with the highest expression foldchange were selected as the
590 candidate genes (Figure 5B). Members of this family regulate chloride transport across the
591 plasma membrane. The *Cyp6a9* involved in the metabolism of insect hormones and in the
592 breakdown of synthetic insecticides (Santisree et al., 2017). *Hsp68* encodes a protein involved in
593 the life-span determination and response to heat shock and starvation (Yang & Lu, 2024). The
594 tumor suppressor protein p53 upregulates the expression of the *CLCA2* genes in response to
595 DNA damage (Walia et al., 2009). The *CLCA2* genes encodes a member of the calcium-activated
596 chloride channel regulator (CLCR) protein family (Walia et al., 2009). The RNA interference of
597 candidate genes confirmed that both *HSP68* and *Cyp6a9* were deeply involved in ovarian
598 function repairment and maintained the egg production, particularly the *HSP68* genes. The
599 weight of egg-laying (0.04289±0.005099, P=0.0003) and the REI (0.2197±0.02745, P=0.0018)
600 in *HSP68* interference group were significantly reduced, indicating that *HSP68* plays a crucial
601 role in the repair of heat damage (Figure 6).
602 This study exposed the engorged female ticks to transient extreme heat (42°C for 30 min), and
603 found that the heat stress did not affect the survival of engorged females, and had only limited
604 effects on reproduction. Based on the microbiome, metabolome and transcriptome analyses, it
605 was confirmed that *H. longicornis* has a series of complex heat stress repair mechanisms (Figure
606 6), and the endosymbionts CLE-Hl and the *HSP68* gene play an important role in heat stress

tolerance of *H. longicornis*. In summary, this study uncovers details for understanding the heat stress tolerance mechanism and ecological adaptability of *H. longicornis*.

DATA AVAILABILITY

The transcriptomic data generated in this study were deposited in the NCBI database (accession number PRJNA1497255), GSA database (accession number CRA046709), and Science Data Bank (https://doi.org/10.57760/sciencedb.j00139.00354.). The metabolomics data were deposited in the OMIX database of China National Center for Bioinformation (OMIX ID OMIX018738) and Science Data Bank (https://doi.org/10.57760/sciencedb.j00139.00354.). The microbiomics data were deposited in the GSA database (accession number CRA046766) and Science Data Bank (https://doi.org/10.57760/sciencedb.j00139.00354.).

ACKNOWLEDGEMENTS

This study was supported by the National Natural Science Foundation of China (No. 31672365, 31272372) and the Postdoctoral Research Foundation of Hebei Normal University (No. L2024B59).

DISCLOSURE

The authors declare no conflict of interest.

ETHICS DECLARATIONS

All experiments were approved by the Animal Ethics Committee of Hebei Normal University (Protocol Number: IACUC-209216).

REFERENCES

627 Amstrup AB, Kovac H, Käfer H, et al. 2024. The heat shock response in *Polistes* spp. brood
628 from differing climates following heat stress. *Journal of Insect Physiology*, **156**: 104667.
629 Bai S, Yao Z, Cai Z, et al. 2025. Bacterial-induced Duox-ROS regulates the Imd immune
630 pathway in the gut by modulating the peritrophic matrix. *Cell Reports*, **44**(3): 115404.
631 Benoit JB, Lopez-Martinez G, Patrick KR, et al. 2011. Drinking a hot blood meal elicits a
632 protective heat shock response in mosquitoes. *Proceedings of the National Academy of*
633 *Sciences of the United States of America* , **108**(19): 8026–8029.
634 Bobrovskikh MA, Gruntenko NE. 2023. Mechanisms of neuroendocrine stress response in
635 *Drosophila* and its effect on carbohydrate and lipid metabolism. *Insects*, **14**(5): 474.
636 Bolger AM, Lohse M, Usadel B. 2014. Trimmomatic: a flexible trimmer for Illumina sequence
637 data. *Bioinformatics*, **30**(15): 2114–2120.
638 Brumin M, Kontsedalov S, Ghanim M. 2011. *Rickettsia* influences thermotolerance in the
639 whitefly *Bemisia tabaci* B biotype. *Insect Science*, **18**(1): 57–66.
640 Buysse M, Plantard O, McCoy KD, et al. 2019. Tissue localization of *Coxiella*-like
641 endosymbionts in three European tick species through fluorescence *in situ* hybridization.
642 *Ticks and Tick-borne Diseases*, **10**(4): 798–804.
643 Calvano MP, Brumatti RC, Garcia MV, et al. 2019. Economic efficiency of *Rhipicephalus*
644 *microplus* control and effect on beef cattle performance in the Brazilian Cerrado.
645 *Experimental and Applied Acarology*, **79**(3-4): 459–471.
646 Caporaso JG, Kuczynski J, Stombaugh J, et al. 2010. QIIME allows analysis of high-throughput
647 community sequencing data. *Nature Methods*, **7**(5): 335–336.

Cibichakravarthy B, Oses-Prieto JA, Ben-Yosef M, et al. 2022. Comparative proteomics of *Coxiella* like endosymbionts (CLEs) in the symbiotic organs of *Rhipicephalus sanguineus* ticks. *Microbiology Spectrum*, **10**(1): e0167321.

Colinet H, Sinclair BJ, Vernon P, et al. 2015. Insects in fluctuating thermal environments. *Annual Review of Entomology*, **60**: 123–140.

Dunbar HE, Wilson AC, Ferguson NR, et al. 2007. Aphid thermal tolerance is governed by a point mutation in bacterial symbionts. *PLoS Biology*, **5**(5): e96.

Duron O, Morel O, Noël V, et al. 2018. Tick-bacteria mutualism depends on B vitamin synthesis pathways. *Current Biology*, **28**(12): 1896–1902.e5.

Duron O, Gottlieb Y. 2020. Convergence of nutritional symbioses in obligate blood feeders. *Trends in Parasitology*, **36**(10): 816–825.

Edgar RC, Haas BJ, Clemente JC, et al. 2011. UCHIME improves sensitivity and speed of chimera detection. *Bioinformatics*, **27**(16): 2194–2200.

Ehlert M, Jagd LM, Braumann I, et al. 2019. Deletion of biosynthetic genes, specific SNP patterns and differences in transcript accumulation cause variation in hydroxynitrile glucoside content in barley cultivars. *Scientific Reports*, **9**(1): 5730.

Ehrenhofer-Murray AE. 2025. Queuine: a bacterial nucleobase shaping translation in eukaryotes. *Journal of Molecular Biology*, **437**(16): 168985.

Fang SM, Zhang Q, Zhang YL, et al. 2021. Heat shock protein 70 family in response to multiple abiotic stresses in the silkworm. *Insects*, **12**(10): 928.

Gao J, Hao Y, Piao X, et al. 2022. Aldehyde dehydrogenase 2 as a therapeutic target in oxidative stress-related diseases: post-translational modifications deserve more attention. *International Journal of Molecular Sciences*, **23**(5): 2682.

671 Ghatta S, Nimmagadda D, Xu X, et al. 2006. Large-conductance, calcium-activated potassium
672 channels: structural and functional implications. *Pharmacology & Therapeutics*, **110**(1):
673 103–116.
674 Gong H, Umemiya R, Zhou J, et al. 2009. Blocking the secretion of saliva by silencing the
675 *HlYkt6* gene in the tick *Haemaphysalis longicornis*. *Insect Biochemistry and Molecular*
676 *Biology*, **39**(5-6): 372–381.
677 Gottlieb Y, Lalzar I, Klasson L. 2015. Distinctive genome reduction rates revealed by genomic
678 analyses of two *Coxiella*-like endosymbionts in ticks. *Genome Biology and Evolution*, **7**(6):
679 1779–1796.
680 Guillén L, Pascacio-Villafán C, Osorio-Paz I, et al. 2022. Coping with global warming: Adult
681 thermal thresholds in four pestiferous *Anastrepha* species determined under experimental
682 laboratory conditions and development/survival times of immatures and adults under natural
683 field conditions. *Frontiers in Physiology*, **13**: 991923.
684 Himler AG, Adachi-Hagimori T, Bergen JE, et al. 2011. Rapid spread of a bacterial symbiont in
685 an invasive whitefly is driven by fitness benefits and female bias. *Science*, **332**(6026): 254–
686 256.
687 Hwang G, Yang DW, Klaudia Geisseova T, et al. 2025. Stress-induced preference for
688 antioxidants by *Drosophila*. *Proceedings of the National Academy of Sciences of the United*
689 *States of America* , **122**(38): e2512852122.
690 Khurshid A, Inayat R, Tamkeen A, et al. 2021. Antioxidant enzymes and heat-shock protein
691 genes of green peach aphid (*Myzus persicae*) under short-time heat stress. *Frontiers in*
692 *Physiology*, **12**: 805509.

King AM, MacRae TH. 2015. Insect heat shock proteins during stress and diapause. *Annual Review of Entomology*, **60**: 59–75.

Li WZ, Zhu T, Zhou JJ, et al. 2022. Effects of short-term heat stress on the activity of three antioxidant enzymes of predatory mite *Neoseiulus barkeri* (acari, phytoseiidae). *Frontiers in Physiology*, **13**: 937033.

Li X, Ma W, Jiang Y. 2023. Honeybees (hymenoptera: apidae) adapt to the shock of high temperature and high humidity through changes in sugars and polyols and free amino acids. *Journal of Insect Science*, **23**(1): 4.

Liu LM, Liu JN, Liu Z, et al. 2013. Microbial communities and symbionts in the hard tick *Haemaphysalis longicornis* (Acari: Ixodidae) from north China. *Parasites & Vectors*, **6**(1): 310.

Lozupone C, Knight R. 2005. UniFrac: a new phylogenetic method for comparing microbial communities. *Applied And Environmental Microbiology*, **71**: 8228–8235.

Ma CS, Ma G, Pincebourde S. 2021. Survive a warming climate: insect responses to extreme high temperatures. *Annual Review of Entomology*, **66**: 163–184.

Madison-Antenucci S, Kramer LD, Gebhardt LL, et al. 2020. Emerging tick-borne diseases. *Clinical Microbiology Reviews*, **33**: e00083–e00118.

McDonald D, Price MN, Goodrich J, et al. 2012. An improved Greengenes taxonomy with explicit ranks for ecological and evolutionary analyses of bacteria and archaea. *The ISME Journal*, **6**(3): 610–618.

Mezouar S, Desnues B, Bechah Y, et al. 2025. Pathogenicity and Virulence of *Coxiella burnetii*: Focus on Q fever. *Virulence*, **16**(1): 2495842.

715 Moustafa MAM, Barnes MM, Wagner NE, et al. 2025. Genome of the invasive North American
716 *Haemaphysalis* longicornis tick as a template for bovine anti-tick vaccine discovery. *BMC*
717 *Genomics*, **26**(1): 307.
718 Noh BE, Kim GH, Lee HS, et al. 2024. The diel activity pattern of *Haemaphysalis longicornis*
719 and its relationship with climatic factors. *Insects*, **15**(8): 568.
720 Oliver KM, Degnan PH, Burke GR, et al. 2010. Facultative symbionts in aphids and the
721 horizontal transfer of ecologically important traits. *Annual Review of Entomology*, **55**: 247–
722 266.
723 Peng X, Feng K, Yang X, et al. 2024. iNAP 2.0: Harnessing metabolic complementarity in
724 microbial network analysis. *iMeta*, **3**(5): e235.
725 Price KJ, Graham CB, Witmier BJ, et al. 2021. Borrelia burgdorferi Sensu Stricto DNA in Field-
726 Collected Haemaphysalis longicornis Ticks, Pennsylvania, United States. *Emerging*
727 *Infectious Diseases*, **27**(2): 608–611.
728 Pruesse E, Quast C, Knittel K, et al. 2007. SILVA: a comprehensive online resource for quality
729 checked and aligned ribosomal RNA sequence data compatible with ARB. *Nucleic Acids*
730 *Research*, **35**(21): 7188–7196.
731 Ren P, Di XY, Yan B, et al. 2025. Impact of short-term high temperature on *Microplitis manilae*
732 (hymenoptera: braconidae) survival, fecundity and progeny development. *Ecology and*
733 *Evolution*, **15**(6): e71626.
734 Sahara A, Nugraheni YR, Patra G, et al. 2019. Ticks (*Acari: Ixodidae*) infestation on cattle in
735 various regions in Indonesia. *Veterinary World*, **12**(11): 1755–1759.

Salvucci ME, Hendrix DL, Wolfe GR. 1999. Effect of high temperature on the metabolic processes affecting sorbitol synthesis in the silverleaf whitefly, *Bemisia argentifolii*. *Journal of Insect Physiology*, **45**(1): 21–27.

Sánchez-Guillén RA, Córdoba-Aguilar A, Hansson B, et al. 2016. Evolutionary consequences of climate-induced range shifts in insects. *Biological Reviews of the Cambridge Philosophical Society*, **91**(4): 1050–1064.

Santisree P, Bhatnagar-Mathur P, Sharma KK. 2017. Heat responsive proteome changes reveal molecular mechanisms underlying heat tolerance in chickpea. *Environmental & Experimental Botany*, **141**: 132–144.

Schloss PD, Westcott SL, Ryabin T, et al. 2009. Introducing mothur: open-source, platform-independent, community-supported software for describing and comparing microbial communities. *Applied And Environmental Microbiology*, **75**: 7537–7541.

Sivan A, Shriram AN, Muruganandam N, et al. 2017. Expression of heat shock proteins (HSPs) in *Aedes aegypti* (L) and *Aedes albopictus* (Skuse) (Diptera: Culicidae) larvae in response to thermal stress. *Acta tropica*, **167**: 121–127.

Smith TA, Driscoll T, Gillespie JJ, et al. 2015. A *Coxiella*-like endosymbiont is a potential vitamin source for the Lone Star tick. *Genome Biology and Evolution*, **7**(3): 831–838.

Sun Y, Yang M, Ye Z, et al. 2024. Effects of high-temperature stress on biological characteristics of *Coccophagus japonicus* compere. *Insects*, **15**(10): 801.

Tian D, Ye RZ, Li YY, et al. 2025. Virome specific to tick genus with distinct ecogeographical distribution. *Microbiome*, **13**(1): 57.

Ventura C, Zinellu E, Maninchedda E, et al. 2003. Dynorphin B is an agonist of nuclear opioid receptors coupling nuclear protein kinase C activation to the transcription of cardiogenic genes in GTR1 embryonic stem cells. *Circulation Research*, **92**(6): 623–629.

Walia V, Ding M, Kumar S, et al. 2009. hCLCA2 is a p53-inducible inhibitor of breast cancer cell proliferation. *Cancer Research*, **69**(16): 6624–6632.

Wang Q, Garrity GM, Tiedje JM, et al. 2007. Naive Bayesian classifier for rapid assignment of rRNA sequences into the new bacterial taxonomy. *Applied And Environmental Microbiology*, **73**(16): 5261–5267.

Wang MF, Zhu D, Dai JF, et al. 2018. Tissue localization and variation of major symbionts in *Haemaphysalis longicornis*, *Rhipicephalus haemaphysaloides*, and *Dermacentor silvarum* in China. *Applied And Environmental Microbiology*, **84**(10): e00029-18.

Wei H, Li X, Tang L, et al. 2020. *16S* rRNA gene sequencing reveals the relationship between gut microbiota and ovarian development in the swimming crab *Portunus trituberculatus*. *Chemosphere*, **254**: 126891.

Westcott SL, Schloss PD. 2017. OptiClust, an improved method for assigning amplicon-based sequence data to operational taxonomic units. *mSphere*, **2**(2): e00073-17.

Williams KD, Helin AB, Posluszny J, et al. 2003. Effect of heat shock, pretreatment and *hsp70* copy number on wing development in *Drosophila melanogaster*. *Molecular Ecology*, **12**(5): 1165–1177.

Xiong S, Yu K, Lin H, et al. 2023. Regulatory network in heat stress response in parasitoid wasp focusing on *Xap5 heat stress regulator*. *iScience*, **27**(1): 108622.

Yang Q, Lu Y. 2024. Heat shock protein 70 genes are involved in the thermal tolerance of *Hippodamia variegata*. *Insects*, **15**(9): 678.

780 Yu XJ, Liang MF, Zhang SY, et al. 2011. Fever with thrombocytopenia associated with a novel
781 bunyavirus in China. *The New England Journal of Medicine*, **364**(16): 1523–1532.
782 Yuan HX, Lv XL, Zhang MQ, et al. 2025. Genetic diversity and expanded epidemic area of
783 novel tick-borne pathogen wetland virus in ticks, wild and domestic animals, and patient in
784 China. *Emerging Microbes & Infections*, **14**(1): 2502003.
785 Zhang CM, Li NX, Zhang TT, et al. 2017. Endosymbiont CLS-HI plays a role in reproduction
786 and development of *Haemaphysalis longicornis*. *Experimental and Applied Acarology*,
787 **73**(3-4): 429–438.
788 Zhang MZ, Bian C, Ye RZ, et al. 2024. A series of patients infected with the emerging tick-
789 borne Yezo virus in China: an active surveillance and genomic analysis. *The Lancet*
790 *Infectious Diseases*, **25**(4): 390–398.
791 Zhang MZ, Bian C, Ye RZ, et al. 2025. Human infection with a novel tickborne Orthonairovirus
792 species in China. *The New England Journal of Medicine*, **392**(2): 200–202.
793 Zhang YK, Zhang XY, Liu JZ. 2019. Ticks (Acari: *Ixodoidea*) in China Geographical
794 distribution, host diversity, and specificity. *Archives of Insect Biochemistry and Physiology*,
795 **102**(3): e21544.
796 Zhong Z, Zhong T, Peng Y, et al. 2021. Symbiont-regulated serotonin biosynthesis modulates
797 tick feeding activity. *Cell Host & Microbe*, **29**(10): 1545–1557.e4.
798 Zhong J. 2012. *Coxiella*-like endosymbionts. *Advances in Experimental Medicine and Biology*,
799 **984**: 365–379.
800 Zhou X, Ling X, Guo H, et al. 2021. *Serratia symbiotica* enhances fatty acid metabolism of *Pea*
801 *aphid* to promote host development. *International Journal of Molecular Sciences*, **22**(11):
802 5951.

803 **FIGURES AND TABLES**

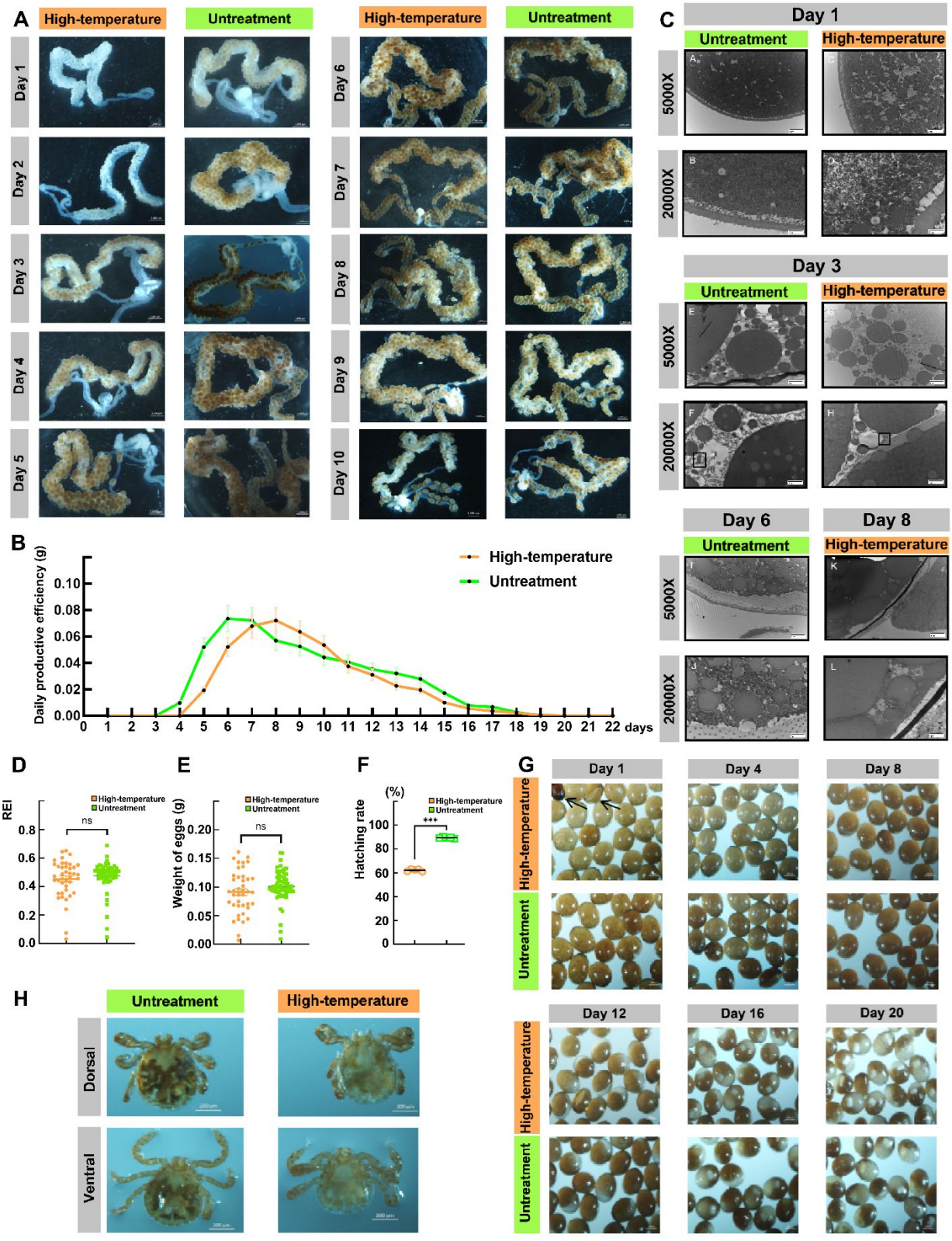

804

Figure 1: Effect of transient extreme heat treatment on reproduction.

A: The effect of transient extreme heat on *Haemaphysalis longicornis* ovarian development by bright-field imaging. The scale bars are 1000 μm in length.

B: The daily productive efficiency of female ticks after transient extreme heat treatment. Data are presented as mean±SEM (n=12).

C: The effect of transient extreme heat on *H. longicornis* ovarian development by TEM. The scale bars are 4 μm (5000×) and 1 μm (20000×) in length.

D: The REI of transient extreme heat treatment and untreatment *H. longicornis*. Data are presented as mean±SEM (n=41). The "ns" indicate the no significant difference (P>0.05) (Student's t-test).

E: The weight of total eggs of transient extreme heat treatment and untreatment *H. longicornis*. Data are presented as mean±SEM (n=41). The "ns" indicate the no significant difference (P>0.05) (Student's t-test).

F: The hatching rates of two groups of eggs. Data are presented as mean±SEM (n=5). The asterisks indicate the significant difference (****P<0.0001) (Student's t-test).

G: The hatching process of two groups of eggs. The scale bars are 500 μm in length.

H: The phenotypes of two groups of offspring generation larvae. The scale bars are 1000 μm in length.

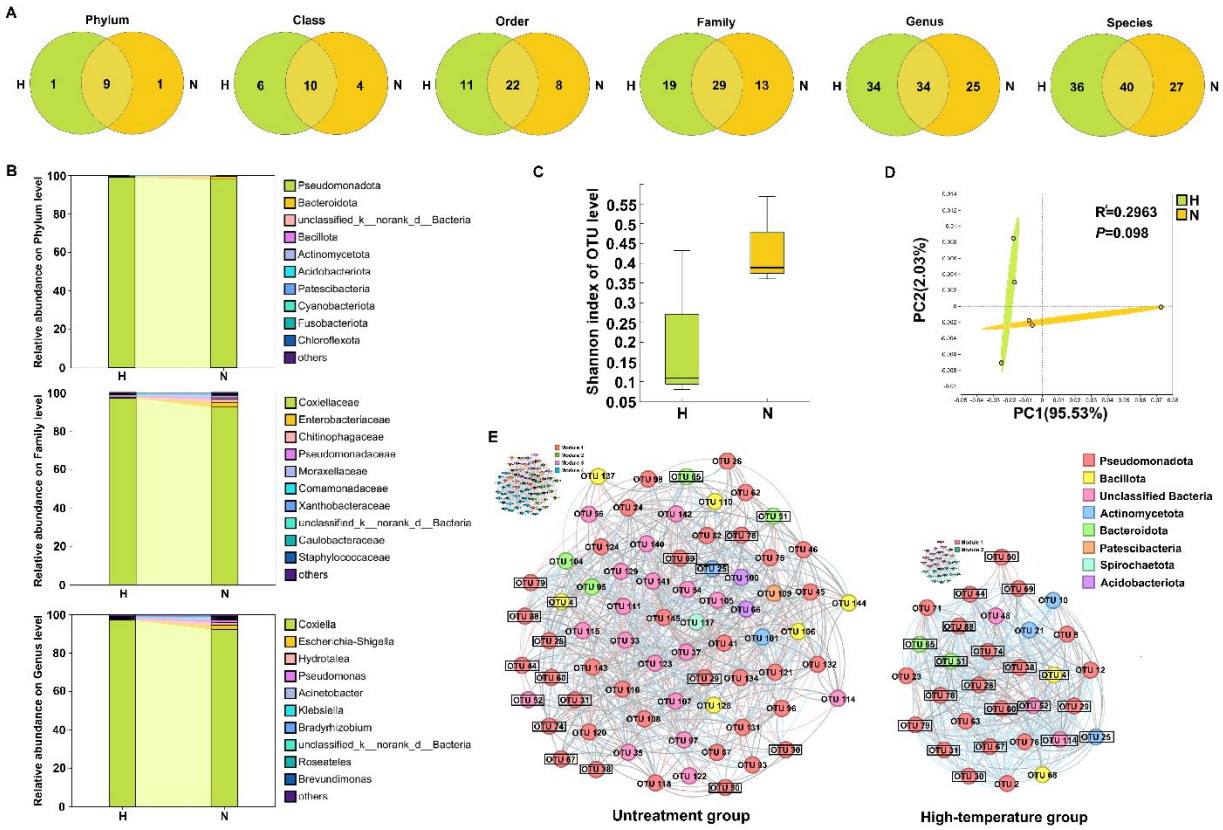

Figure 2: Effect of transient extreme heat on ovarian microbiota of *Haemaphysalis longicornis*.

A: The venn diagram of ovarian OTUs between the untreatment group and high-temperature group at the phylum, class, order, family, genus and species levels.

B: The proportions of the top 10 dominant bacteria in untreatment group and high-temperature group at the phylum, family, and genus levels.

C: The bacterial community diversity (Shannon index) of ovarian microbiota between the untreatment group and high-temperature group.

D: Principal coordinate analysis (PCoA) results of the ovarian microbiota in untreatment group and high-temperature group.

835 E: The co-occurrence network of ovarian microbiota between the untreatment group and high-
836 temperature group. The thumbnail in left corner represents coloring according to the modules.
837 The black boxes marked the mutual OTU in the untreatment group and high-temperature group.
838 The nodes colour in main image stands for the phylum of OTUs.

839 H stands for the high-temperature group, and N stands for the untreatment group.

840

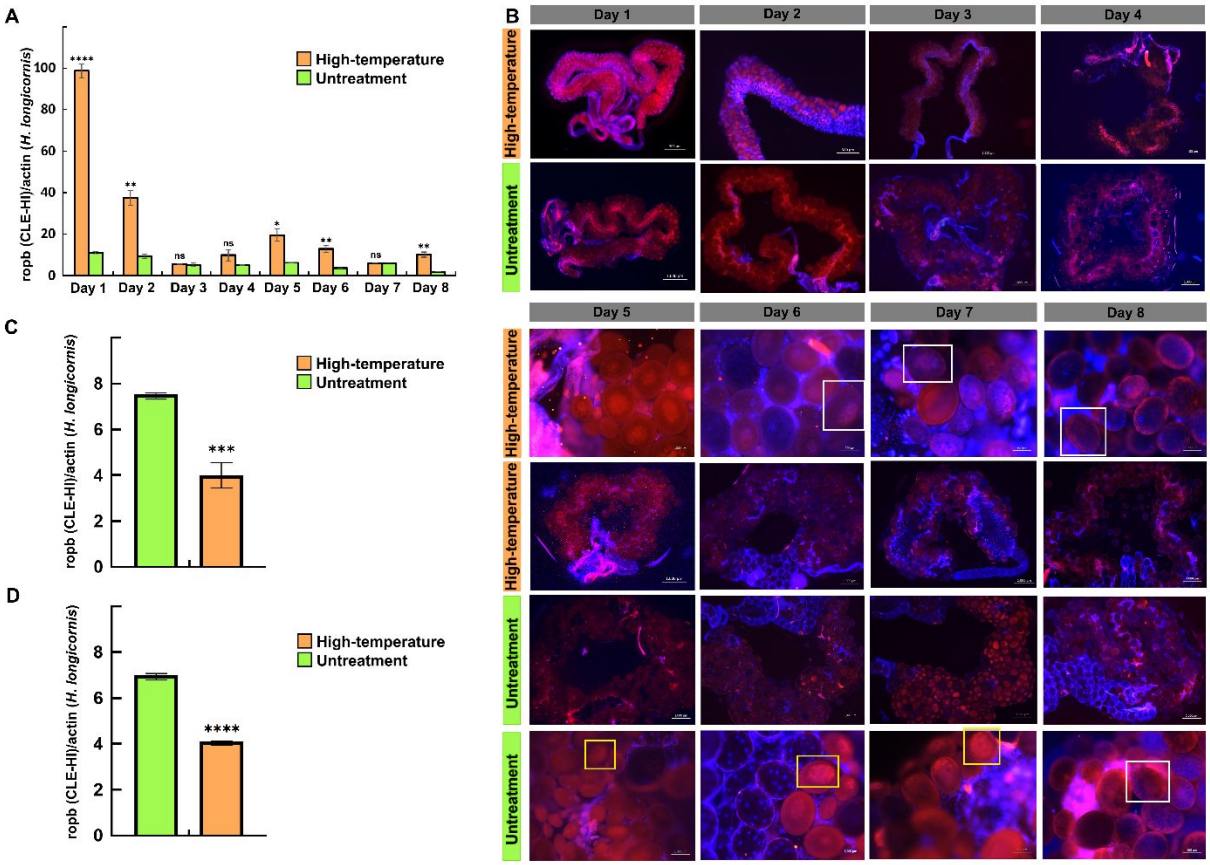

Figure 3: Effect of transient extreme heat on ovarian CLE-Hl.

A: The relative amounts of ovarian CLE-Hl in two groups. Data are presented as mean±SEM (*n*=3). The "ns" indicate the no significant difference (*P*>0.05). And the asterisks indicate the significant difference (0.01≤**P*<0.05, 0.001≤***P*<0.01, 0.0001≤****P*<0.001, and *****P*<0.0001) (Student's *t*-test).

B: Spatiotemporal expression pattern of the CLE-Hl distribution in two groups measured by DNA-fluorescence in situ hybridization. The scale bars are 1000 μm, 500 μm and 200 μm in length.

C: The relative amounts of eggs' CLE-Hl in two groups. Data are presented as mean±SEM (*n*=3). The asterisks indicate the significant difference (0.01≤**P*<0.05, 0.001≤***P*<0.01, 0.0001≤****P*<0.001, and *****P*<0.0001) (Student's *t*-test).

853 D: The relative amounts of offspring generation larval CLE-Hl in two groups. Data are presented
854 as mean±SEM (*n*=3). The asterisks indicate the significant difference (****P<0.0001) (Student's
855 *t*-test).

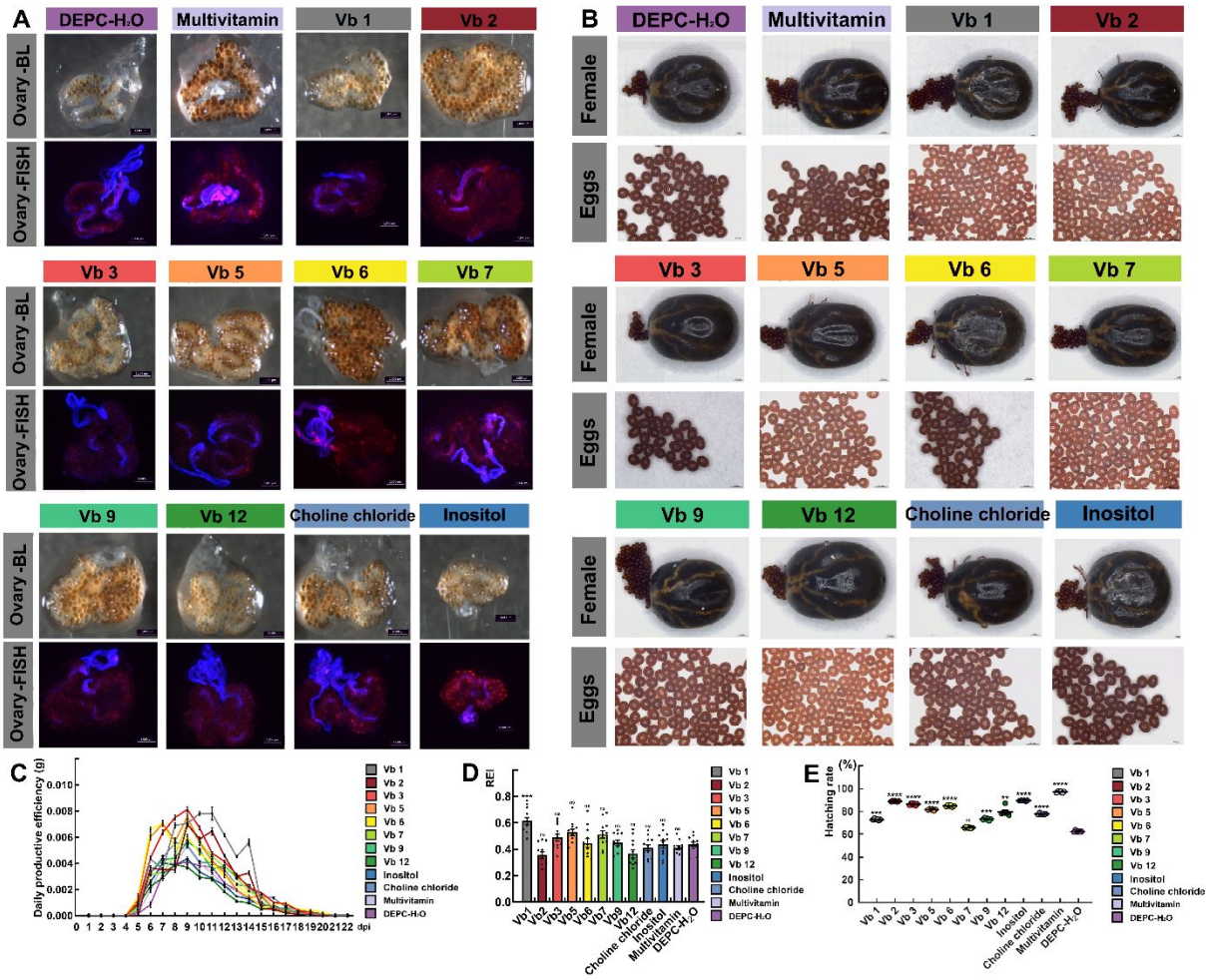

Figure 4: Effect of Vitamin B rescue female ticks in transient extreme heat treatment.

A: The bright-field images and the spatiotemporal expression pattern of the CLE-Hl distribution in Vitamin B rescue ticks ovarian after transient extreme heat treatment. The scale bars are 1000 μm in length.

B: The appearances of ticks and eggs in Vitamin B rescue groups after transient extreme heat treatment. The scale bars are 1mm and 500 μm in length.

C: The daily productive efficiency of Vitamin B rescue female ticks after transient extreme heat treatment. Data are presented as mean±SEM (*n*=12).

865 D: The REI of Vitamin B rescue female ticks after transient extreme heat treatment. Data are
866 presented as mean±SEM (n=12). The “ns” indicate the no significant difference (P>0.05). And
867 the asterisks indicate the significant difference (0.0001≤***P<0.001) (Tukey’s test).
868 E: The hatching rates of eggs in Vitamin B rescue groups after transient extreme heat treatment.
869 Data are presented as mean±SEM (n=6). The “ns” indicate the no significant difference
870 (P>0.05). And the asterisks indicate the significant difference (0.001≤**P<0.01,
871 0.0001≤***P<0.001, and ****P<0.0001) (Tukey’s test).
872

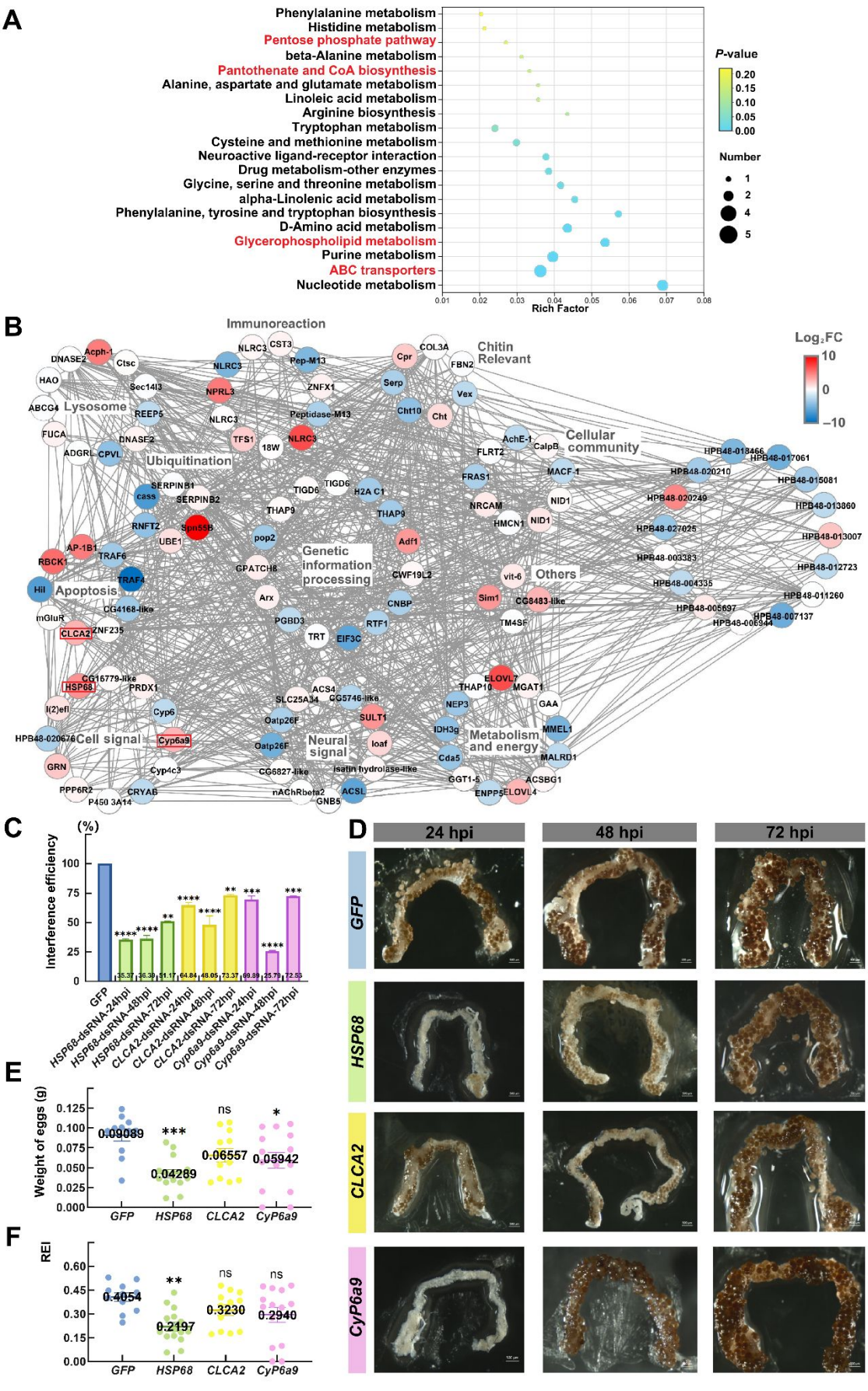
A
Phenylalanine metabolism
Histidine metabolism
Pentose phosphate pathway
beta-Alanine metabolism
Pantothenate and CoA biosynthesis
Alanine, aspartate and glutamate metabolism
Linoleic acid metabolism
Arginine biosynthesis
Tryptophan metabolism
Cysteine and methionine metabolism
Neuroactive ligand-receptor interaction
Drug metabolism-other enzymes
Glycine, serine and threonine metabolism
alpha-Linolenic acid metabolism
Phenylalanine, tyrosine and tryptophan biosynthesis
D-Amino acid metabolism
Glycerophospholipid metabolism
Purine metabolism
ABC transporters
Nucleotide metabolism
Rich Factor
P-value
Number
B
Immunoreaction
Chitin Relevant
Cellular community
Lysosome
Ubiquitination
Genetic information processing
Others
Apoptosis
Cell signal
Neural signal
Metabolism and energy
Log2FC
C
Interference efficiency
(%)
GFP
HSP68-dsRNA-24hpi
HSP68-dsRNA-48hpi
HSP68-dsRNA-72hpi
CLCA2-dsRNA-24hpi
CLCA2-dsRNA-48hpi
CLCA2-dsRNA-72hpi
Cyp6a9-dsRNA-24hpi
Cyp6a9-dsRNA-48hpi
Cyp6a9-dsRNA-72hpi
D
24 hpi
48 hpi
72 hpi
GFP
HSP68
CLCA2
CyP6a9
E
Weight of eggs (g)
0.09089
0.04289
0.06557
0.05942
GFP
HSP68
CLCA2
CyP6a9
F
REI
0.4054
0.2197
0.3230
0.2940
GFP
HSP68
CLCA2
CyP6a9

Figure 5: Transient extreme heat response of *Haemaphysalis longicornis* revealed by metabonomics and transcriptomics.

A: The KEGG pathway enrichment of different metabolites between the high-temperature group and the untreatment group. For each dot in diagram, the *P*-value of enriched pathways is indicated by a color gradient; the amounts of enriched metabolites in each pathway are indicated by the size of the dot.

B: The interaction network of differentially expressed genes based on the KEGG database. For each dot in diagram, the Log_2FC of enriched genes are indicated by a color gradient.

C: The relative expression of genes (*GFP*, *HSP68*, *CLCA2*, *CyP6a9*) at 24 h, 48 h and 72h after RNA interference was compared. Data are presented as mean±SEM (n=3). The asterisks indicate the significant difference (0.0001≤***P<0.001, and ****P<0.0001) (Tukey's test).

D: The effect of *H. longicornis* ovarian development in candidate genes (*GFP*, *HSP68*, *CLCA2*, *CyP6a9*) knockdown groups measured by bright-field imaging after transient extreme heat treatment. The scale bars are 1000 μm in length.

E: The weight of total eggs of candidate genes (*GFP*, *HSP68*, *CLCA2*, *CyP6a9*) knockdown groups after transient extreme heat treatment of *H. longicornis*. Data are presented as mean±SEM (n=12). The "ns" indicate the no significant difference (P>0.05). And the asterisks indicate the significant difference (0.001≤**P<0.01) (Tukey's test).

F: The REI of candidate genes (*GFP*, *HSP68*, *CLCA2*, *CyP6a9*) knockdown groups after transient extreme heat treatment of *H. longicornis*. Data are presented as mean±SEM (n=12). The "ns" indicate the no significant difference (P>0.05). And the asterisks indicate the significant difference (0.01≤*P<0.05, and 0.0001≤***P<0.001) (Tukey's test).

896 *GFP* stands for *green fluorescent protein*, *HSP68* stands for *heat shock protein 68*, *CLCA2*

897 stands for *chloride channel accessory 2*, *CyP6a9* stands for *cytochrome P450 6a9*.

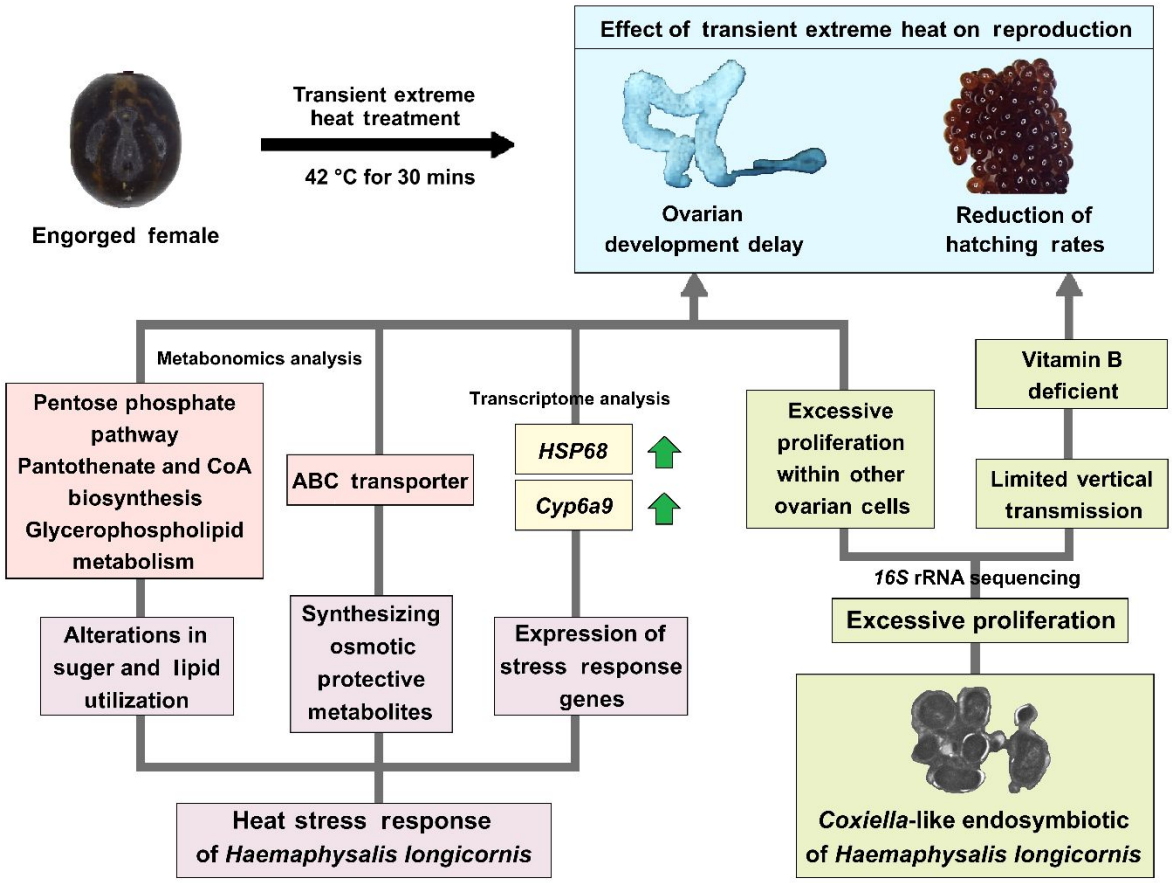

Figure 6: Schematic diagram of the *H. longicornis* heat stress response mechanism.

Summary diagram showing the heat stress response mechanisms in multiaspects of *H. longicornis*. The metabonomics analysis revealed that the "pentose phosphate pathway", "pantothenate and CoA biosynthesis", and "glycerophospholipid metabolism" enriched pathways are associated with alterations in sugar and lipid utilization, while the "ABC transporter" enriched pathway is involved in typical osmotic protective metabolites synthesis, with the purpose of protecting cell structure stability. The transcriptome analysis revealed that the *HSP68* and *Cyp6a9* genes are involved in heat stress response. The *16S rRNA* sequencing and further research of CLE-Hl revealed that the excessive proliferation of CLE-Hl in other ovarian cells is also involved in heat stress response, and limited vertical transmission of CLE-Hl reduced the hatching rate of offspring.

910 *HSP68* stands for *heat shock protein 68*, *CyP6a9* stands for *cytochrome P450 6a9*.

911

912 **Table 1 The co-occurrence network details of the untreatment group and high-temperature**

913 **group.**

	untreatment group	high-temperature group
Description Length	574.771	1 797.861
Number of Communities	15	33
Modularity	0.112	0.165
Modularity with resolution	0.112	0.165
Number of Communities	2	4
Number of Weakly Connected Components	1	1
Average Clustering Coefficient	0.789	0.29
Total triangles	2 022	1 228
Average Degree	22.645	18.845
Average Weighted Degree	22.645	18.845
Density	0.755	0.269
Diameter	2	3
Radius	2	2
Average Path length	1.245161	1.74004

914

915 **Table 2 The Top 10 OTUs' closeness centrality of the untreatment group and high-**

916 **temperature group.**

Top 10 OUTs of the untreatment group	Closeness centrality	Top 10 OUTs of the high-temperature group	Closeness centrality
OTU123	0.660377358	OTU60	0.909090909
OTU41	0.642201835	OTU74	0.882352941
OTU107	0.636363636	OTU28	0.882352941
OTU140	0.636363636	OTU51	0.857142857
OTU108	0.630630631	OTU63	0.857142857
OTU116	0.630630631	OTU38	0.857142857
OTU143	0.630630631	OTU78	0.857142857
OTU121	0.630630631	OTU65	0.833333333
OTU35	0.630630631	OTU31	0.833333333
OTU45	0.625000000	OTU67	0.833333333

917 **SUPPORTING INFORMATION**

918 Additional supporting information may be found online in the Supporting Information section at

919 the end of the article.

920

Supplementary Information

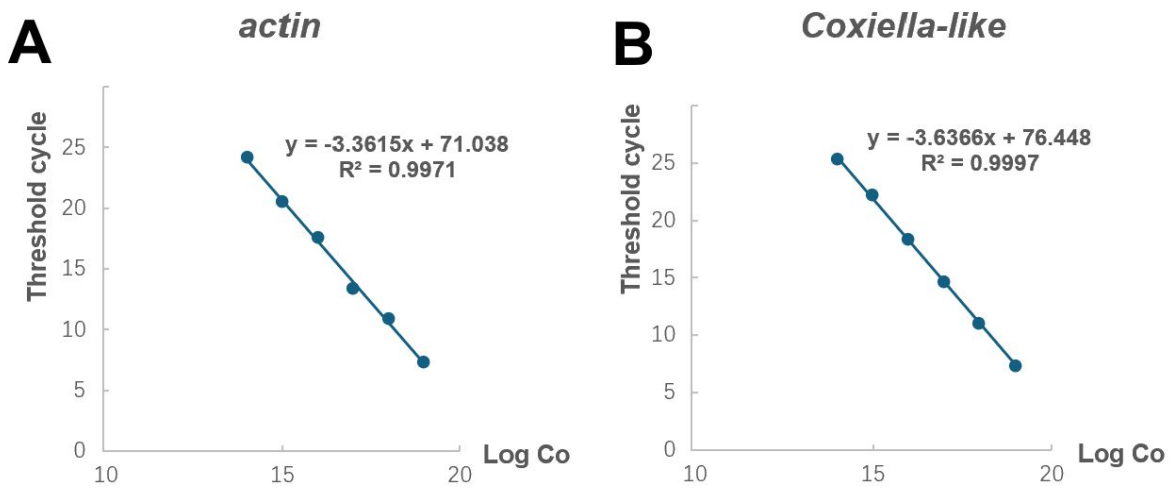

Supplemental Figure S1: Standard curve for qPCR

A) Standard curve of *H. longicornis actin*. B) Standard curve of CLS-Hl *ropb*.

Log Co: The log value of the copy number concentration of the standard; Threshold Cycle: The number of cycles required for the sample concentration to reach a certain threshold.

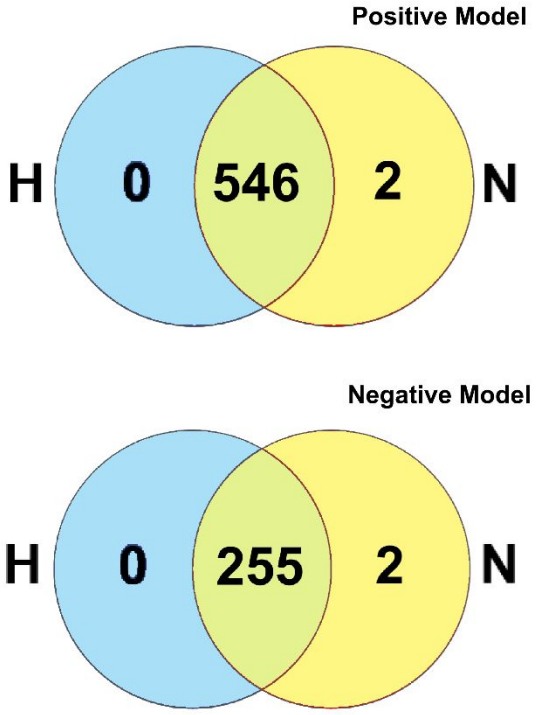

928
929 **Supplemental Figure S2: The venn diagram of ovarian metabolites between the high-temperature**

930 **group and the untreatment group in positive and negative model.**

931 H stands for the high-temperature group, and N stands for the untreatment group.

932

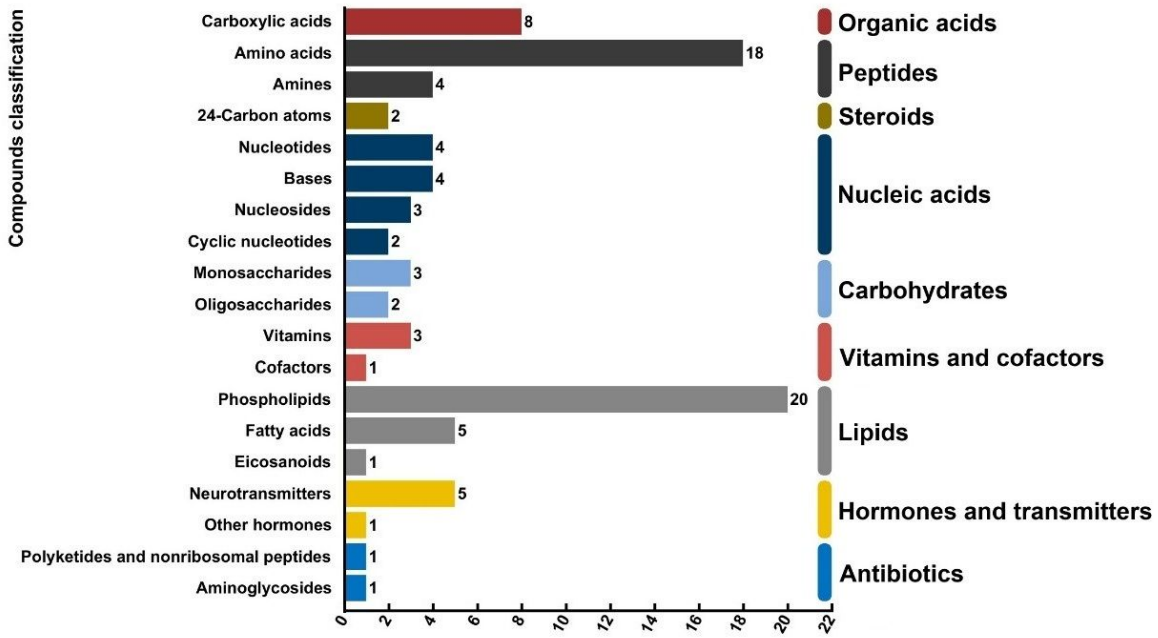

933

934 **Supplemental Figure S3: The metabolites annotated in the KEGG database.**

935 The annotated metabolites were classified in organic acids, peptides, steroids, nucleic acids,

936 carbohydrates, vitamins and cofactors, hormones and transmitters, lipids and antibiotics.

937

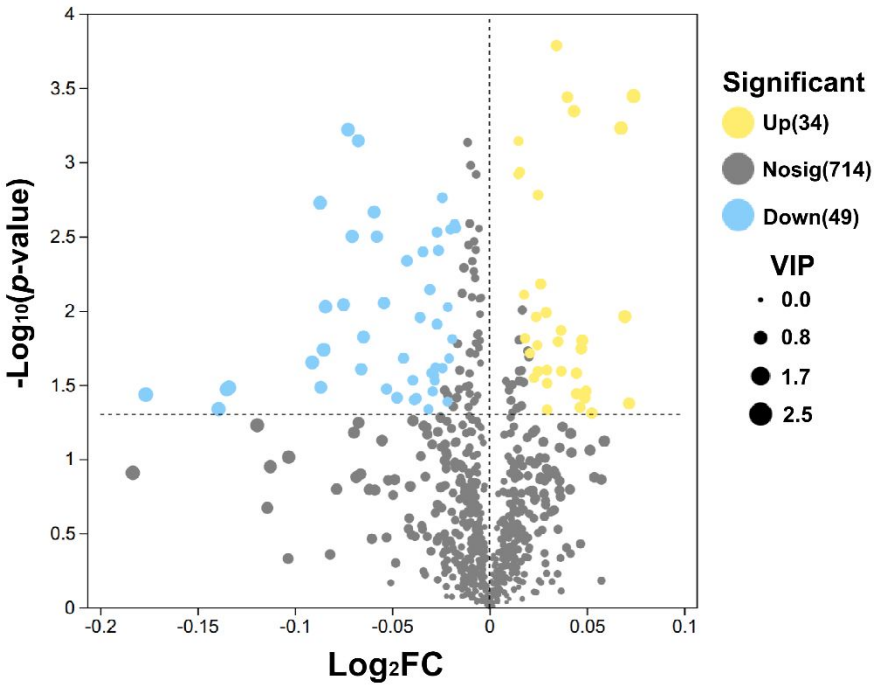

Supplemental Figure S4: The volcano map of different metabolites between the high-temperature group and the untreatment group.

For each dot in volcano map, the significance of metabolites are indicated by a color, yellow stands for the significantly up-regulation, and blue stands for the significantly down-regulation. The VIP-value of metabolite is indicated by the size of the dot.

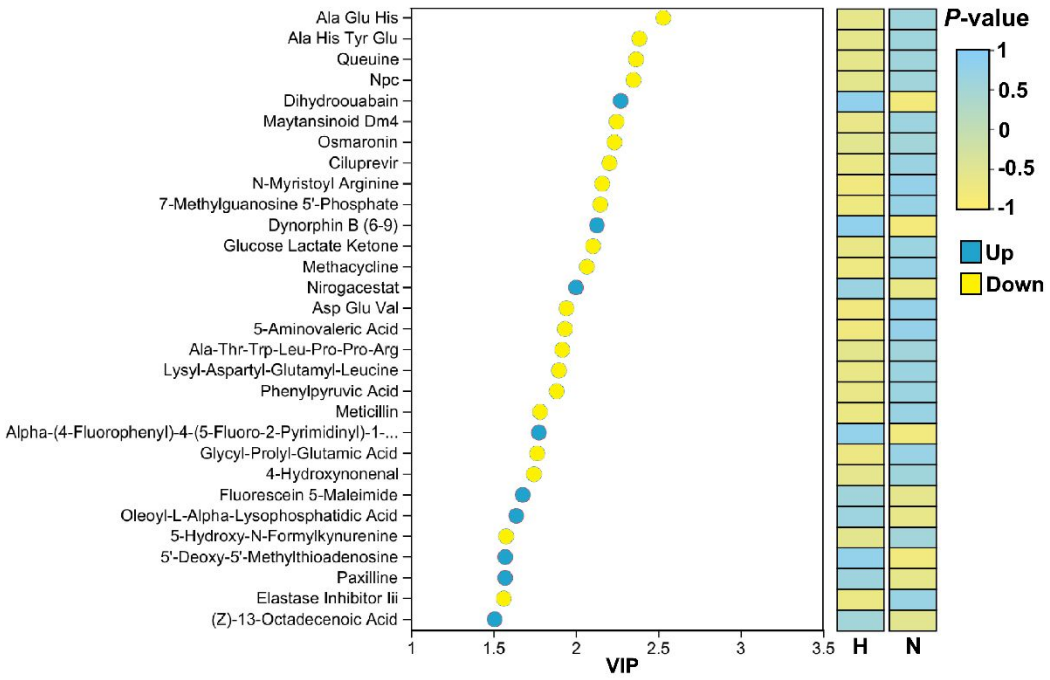

945

946 **Supplemental Figure S5: The VIP diagram of different metabolites between the high-temperature**

947 **group and the untreatment group.**

948 For each dot in VIP diagram, the significance of metabolites are indicated by a color, yellow stands for

949 the significantly up-regulation, and blue stands for the significantly down-regulation; the *P*-value of

950 metabolite is indicated by a color gradient.

951

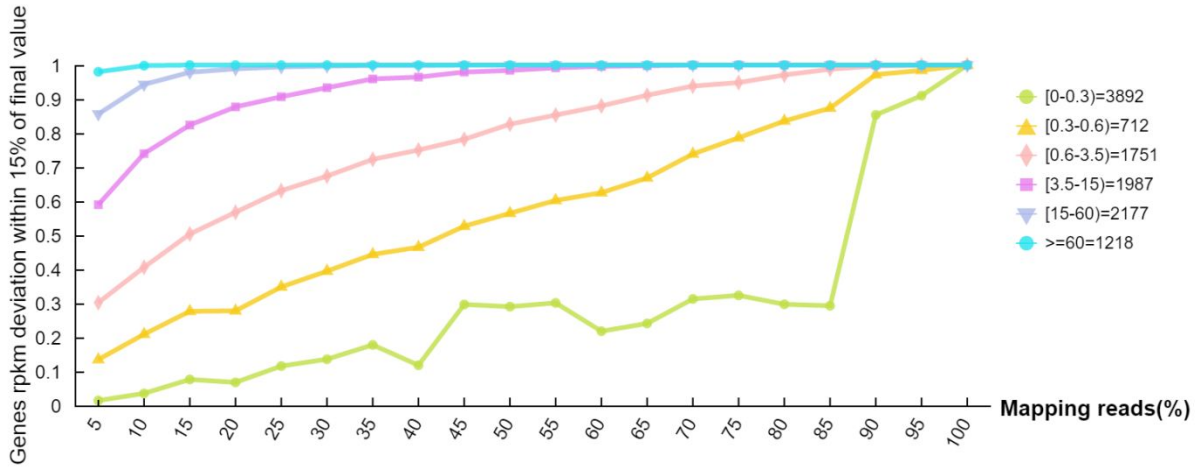

Supplemental Figure S6: The sequencing saturation curve.

The abscissa is the percentage of valid reads. The ordinate is the proportion of deviation between the expression and the final value under the sampling condition.

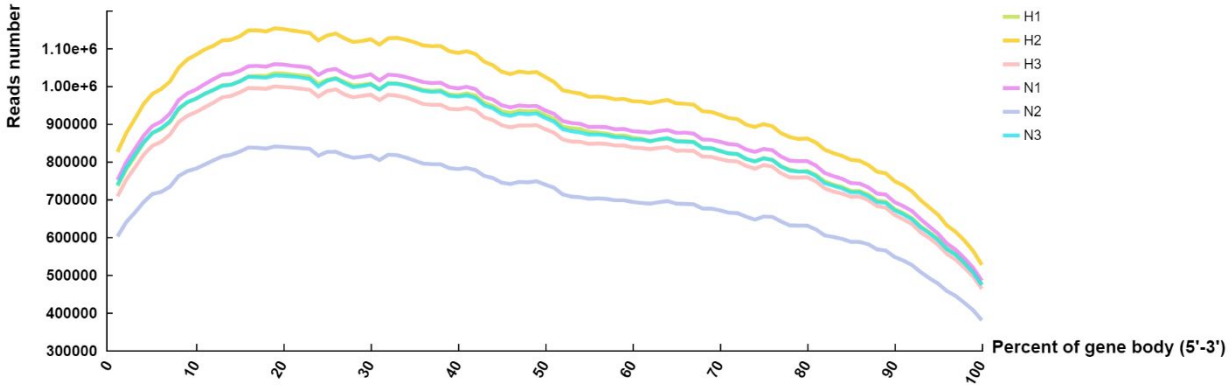

958

959 **Supplemental Figure S7: The sequencing coverage distribution.**

960 The horizontal coordinate is the percentage of the base length of a single gene to the total base length, 0

961 represents the 5' end of the gene, 100 represents the 3' end of the gene; The ordinate is the sum of the

962 number of sequences aligned to the corresponding interval on the horizontal axis of all genes. The H1, H2

963 and H3 stands for the sample of the high-temperature group at the 3 dpt, and the N1, N2 and N3

964 stands for the sample of the untreatment group at the 3 dpt.

965

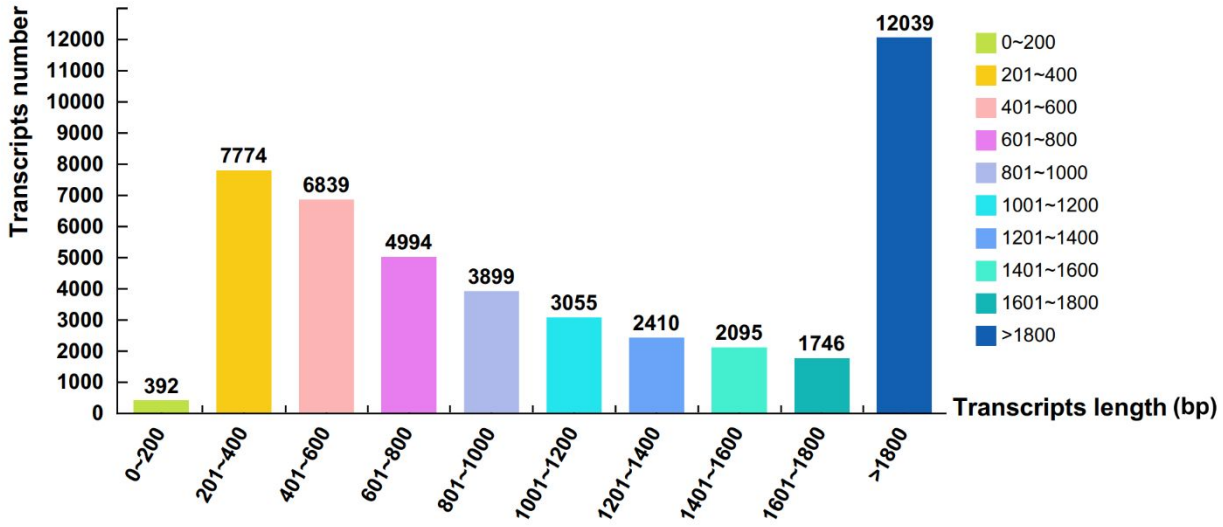

966

967 **Supplemental Figure S8: Distribution of transcript length.**

968 Distribution of different transcript lengths. The horizontal coordinate is the length range of transcript; The

969 ordinate is the number of transcripts within the length range of the transcript.

970

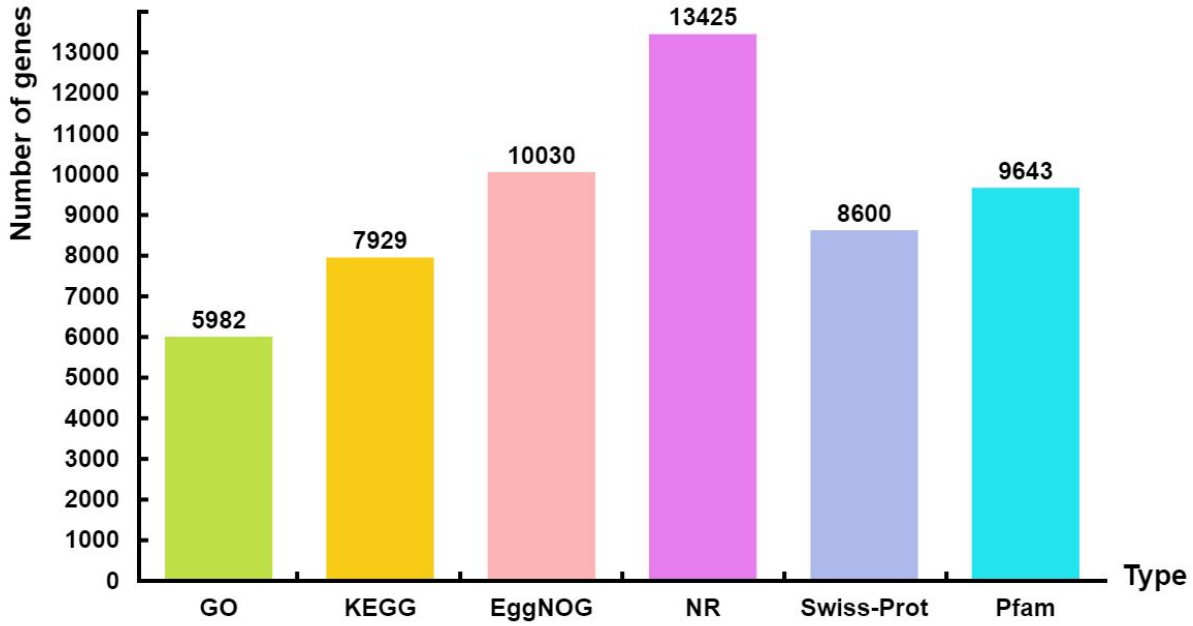

971

972 **Supplemental Figure S9: Functional annotation statistics of transcripts.**

973 The horizontal coordinate indicates the database name; The ordinate represents the number or percentage

974 of sequences annotated to the database.

975

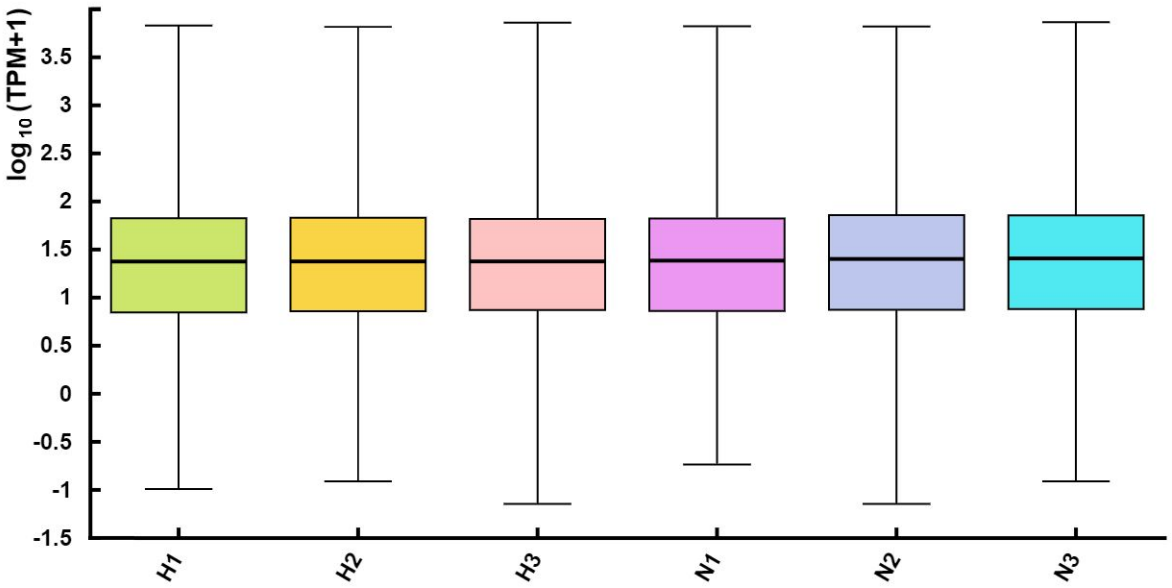

976

977 **Supplemental Figure S10: Distribution of transcription expression in six samples.**

978 The H1, H2 and H3 stands for the sample of the high-temperature group at the 3 dpt, and the N1, N2

979 and N3 stands for the sample of the untreatment group at the 3 dpt.

980

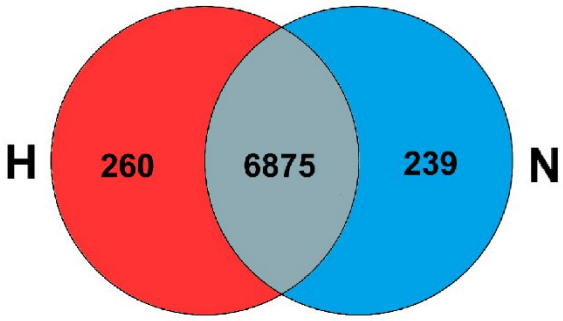

Supplemental Figure S11: The venn diagram of the high-temperature and untreatment group expression genes.

H stands for the high-temperature group, and N stands for the untreatment group.

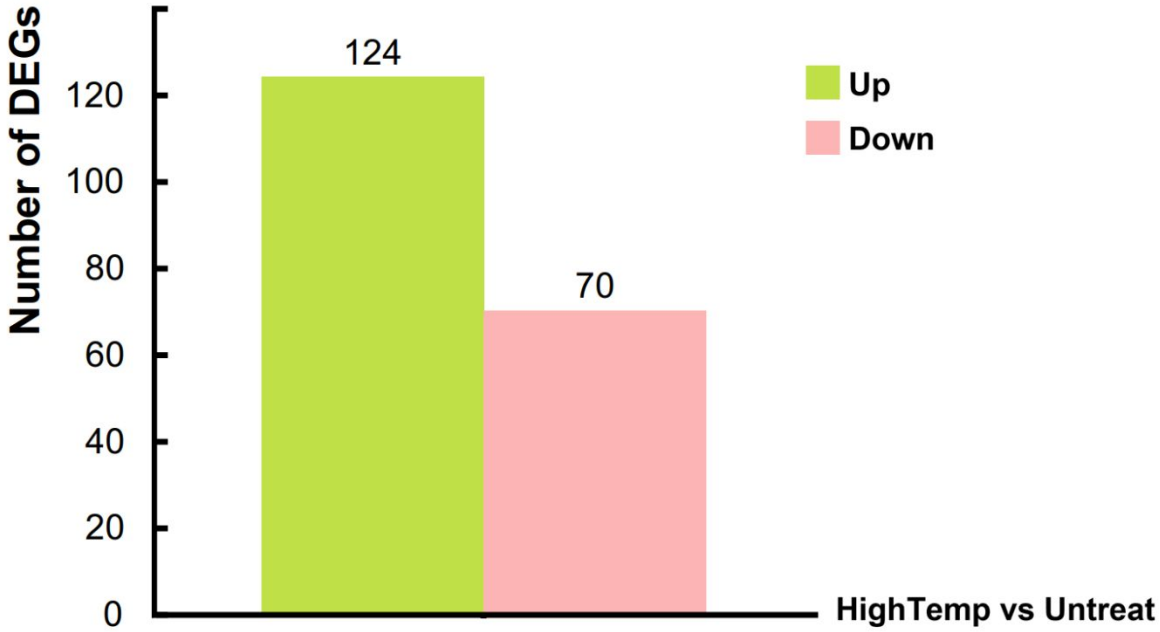

986

987 **Supplemental Figure S12: The amount of different expression gene between the high-temperature**

988 **group and the untreatment group.**

989 The green stands for the number of up-regulated genes, and the pink stands for the number of down-

990 regulated genes.

991

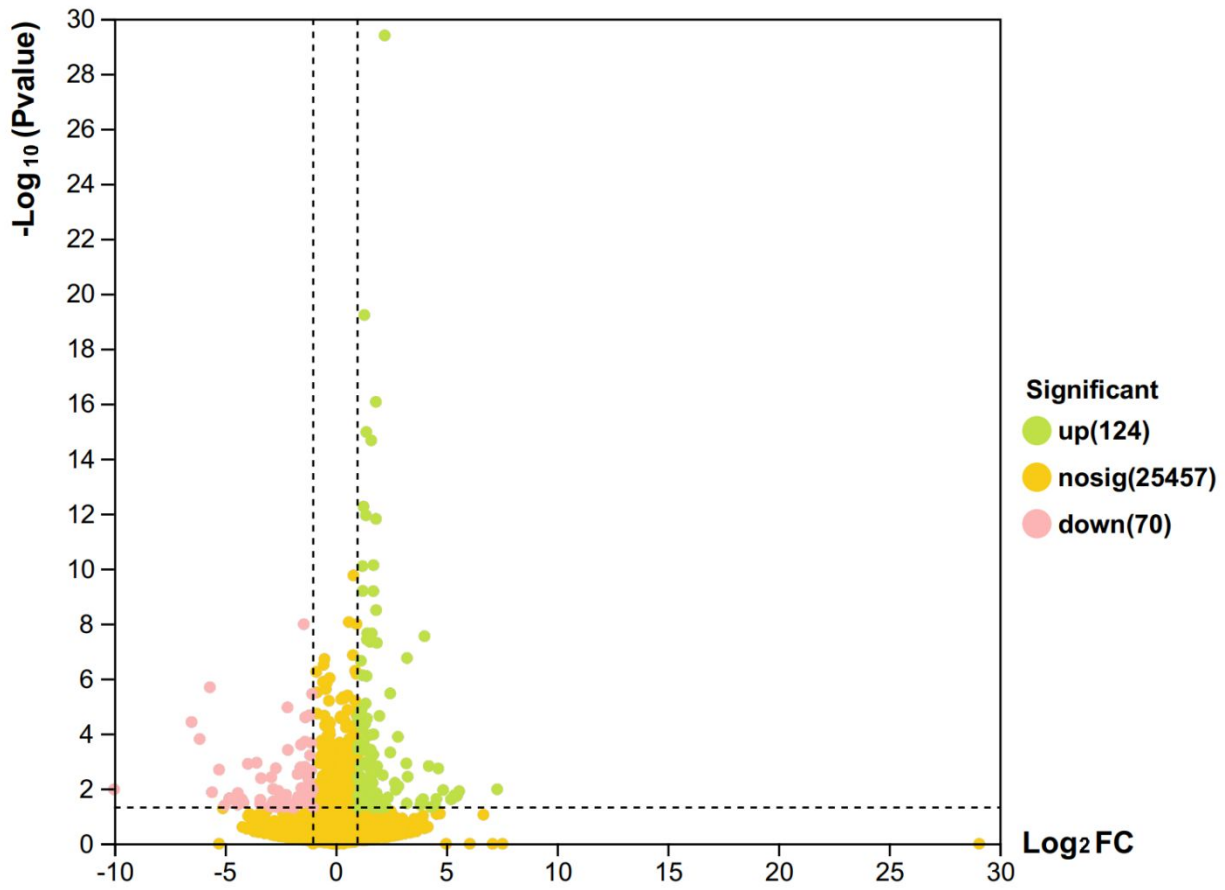

992

993 **Supplemental Figure S13: The volcano map of different expression gene between the high-**

994 **temperature group and the untreatment group.**

995 Each dot stands for a specific gene, with the green dots representing significantly up-regulated genes,

996 pink dots representing significantly down-regulated genes, and the yellow dots representing non-

997 significantly differenced genes.

998

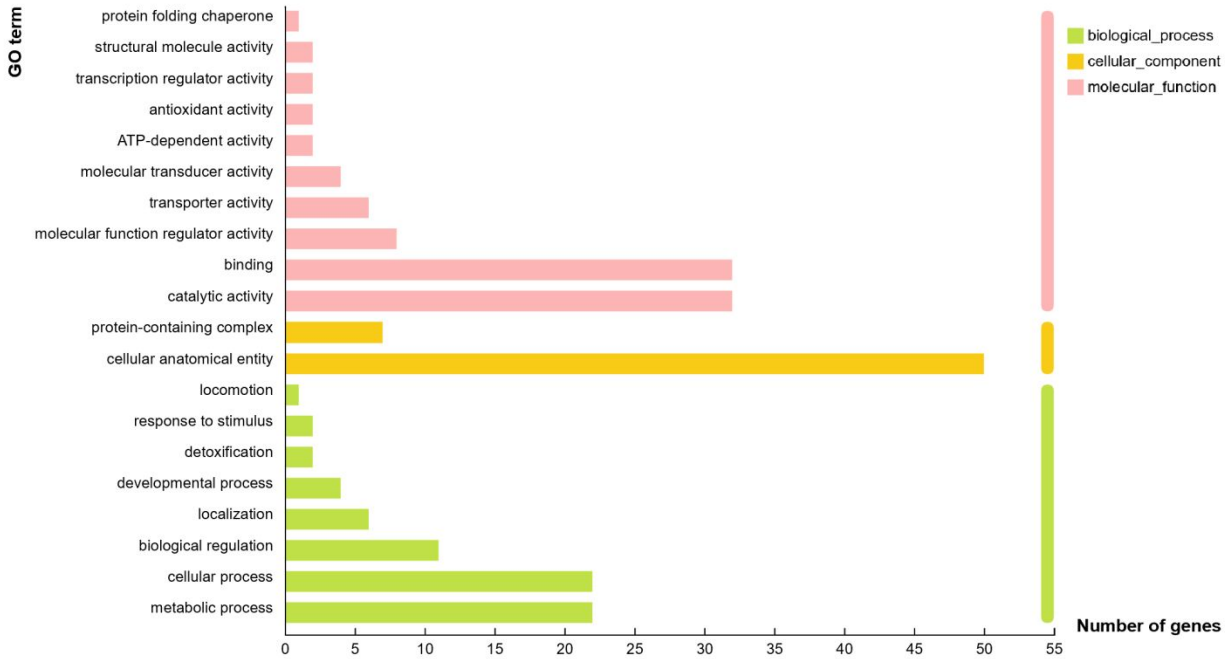

Supplemental Figure S14: The Column chart of GO classification statistics.

The ordinate indicates the secondary classification term for GO, and the abscise indicates the number of genes/transcripts compared to that secondary classification.

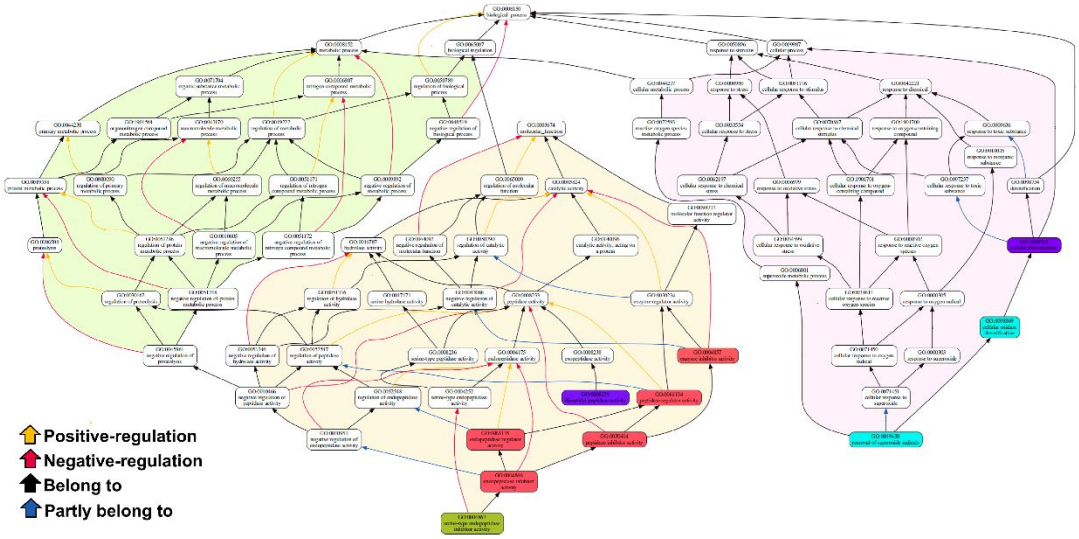

Supplemental Figure S15: The directed acyclic graph based on the GO database.

For each arrow in diagram, the relationship of GO term is indicated by a color, yellow stands for the positive-regulation, red stands for the negative-regulation, black stands for the belong to, and nevy blue stands for the partly belong to.

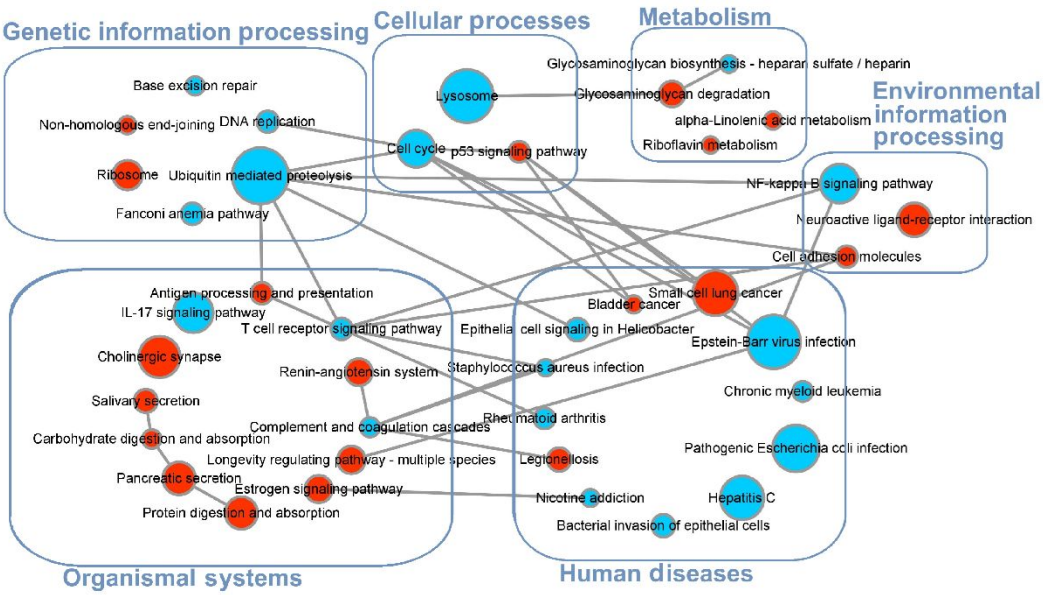

Supplemental Figure S16: The GSEA analysis diagram of differentially expressed genes based on the KEGG database.

For each dot in diagram, the significance of enriched pathway is indicated by a color, red stands for the significantly up-regulation, and blue stands for the significantly down-regulation.

Supplementary Table S1 The concentration in the Vitamin B rescue after transient extreme heat treatment.

Name	Concentration (μg/mL)
Vitamin B1	100
Vitamin B2	20
Vitamin B3	100
Vitamin B5	100
Vitamin B6	100
Vitamin B7	1
Vitamin B9	30
Vitamin B12	1
Choline chloride	185
Inositol	118
Multivitamin	mixture of above vitamins

1019 **Supplementary Table S2 The sequence of primers**

Name	Sequence (5′-3′)
rpoB-F	CCTTATTTAGAAGACGGGACTC
rpoB-R	ATTACCCATACCTTTTGCTG
Actin-F	CGTTCCTGGGTATGGAATCG
Actin-R	TCCACGTCGCACTTCATGAT
HSP68-F-T7	GGATCCTAATACGACTCACTATAGGAGGTCGAAGATGAGCACGTT
HSP68-F	AGGTCGAAGATGAGCACGTT
HSP68-R	GCTACGACGACCCCAAGAT
HSP68-R-T7	GGATCCTAATACGACTCACTATAGGGCTACGACGACCCCAAGAT
CLCA2-F-T7	GGATCCTAATACGACTCACTATAGGGTCGTCGTGAAGCGTGATG
CLCA2-F	GTCGTCGTGAAGCGTGATG
CLCA2-R	AACGCTCTTCTATTTCCAGGC
CLCA2-R-T7	GGATCCTAATACGACTCACTATAGGAACGCTCTTCTATTTCCAGGC
Cyp6a9-F-T7	GGATCCTAATACGACTCACTATAGGGCATCACCGCCTTCATTTTC
Cyp6a9-F	GCATCACCGCCTTCATTTTC
Cyp6a9-R	ATACCAGGACCACCGATTGA
Cyp6a9-R-T7	GGATCCTAATACGACTCACTATAGGATACCAGGACCACCGATTGA
HSP68-qPCR-F	GCCAAGACGTTCACCACGTA
HSP68- qPCR-R	GTTGGTGATGCGGATGCTCT
CLCA2- qPCR-F	TTCTGGTGGACGCCAATCTC
CLCA2- qPCR-R	TGCACGTCCTTGGTACACTC
Cyp6a9- qPCR-F	GAAGTGCAGAAGAACCCGGA
Cyp6a9- qPCR-R	AATGTGGTAGGCGGTTTCGT

1020

Supplementary Table S3 The operational taxonomic units (OTUs) clustering analysis of the high-temperature group and the untreatment group.

The data was presented in a separate Excel.

Supplementary Table S4 All operational taxonomic units (OTUs) in phylum, class, order, family, genus, and species levels.

The data was presented in a separate Excel.

Supplementary Table S5 The quality control results of ovarian transcriptome analysis in the high-temperature group and the untreatment group.

Sample	Clean reads	Clean bases	Error rate (%)	Q20 (%)	Q30 (%)	GC content (%)
H1	62 155 726	9 338 805 831	0.0117	98.93	96.54	52.19
H2	69 373 622	10 422 264 577	0.0117	98.92	96.49	52.27
H3	60 030 048	9 013 581 692	0.0117	98.92	96.50	52.03
N1	65 061 108	9 770 807 879	0.0117	98.94	96.55	51.94
N2	49 125 028	7 388 244 375	0.0118	98.86	96.31	52.02
N3	62 229 806	9 347 590 840	0.0118	98.90	96.42	51.87

1032 **Supplementary Table S6 The comparative analysis of ovarian transcriptome sequences in the high-**

1033 **temperature group and the untreatment group.**

Sample	Total reads	Total mapped	Multiple mapped	Uniquely mapped
H1	62 155 726	49 597 735 (79.80%)	1 431 486 (2.30%)	48 166 249 (77.49%)
H2	69 373 622	55 397 900 (79.85%)	1 534 249 (2.21%)	53 863 651 (77.64%)
H3	60 030 048	47 762 640 (79.56%)	1 315 244 (2.19%)	46 447 396 (77.37%)
N1	65 061 108	51 838 094 (79.68%)	1 384 118 (2.13%)	50 453 976 (77.55%)
N2	49 125 028	39 145 842 (79.69%)	1 007 771 (2.05%)	38 138 071 (77.63%)
N3	62 229 806	49 565 137 (79.65%)	1 226 476 (1.97%)	48 338 661 (77.68%)

1034

短暂极端热胁迫下长角血蜱雌蜱的生殖适应机制

作者

李凤佼[1,2,#]，齐丹琳[1,#]，刘敬泽[1,*]

作者单位

[1]分子细胞生物学教育部重点实验室，河北省动物生理生化与分子生物学重点实验室，河北省细胞生物学基础学科研究中心，河北省生态环境协同创新中心，河北师范大学生命科学学院，石家庄，河北 050024，中国

[2]生态学博士后科研流动站，河北师范大学生命科学学院，石家庄，河北 050024，中国

通讯作者:

刘敬泽： liujingze@hebtu.edu.cn; https://orcid.org/0000-0002-0923-1775

摘要

全球气候变化导致极端高温事件频发且强度显著增加，此类事件对节肢动物的个体生存和种群延续构成威胁。长角血蜱（*Haemaphysalis longicornis*）是一类吸血节肢动物，主要分布于亚洲。由于长角血蜱具有极强的生态适应能力，其分布范围不断扩大，现已成功入侵至多个地区。野外调查证实长角血蜱可耐受 5.7°C 至 42.1°C 的环境温度，但其高温胁迫响应机制尚未被详细探究。为揭示长角血蜱的高温耐受机制和生态适应能力，本研究对饱血雌蜱进行了短暂的极端高温胁迫（42°C 持续 30 分钟），结果发现高温胁迫并未影响饱

血雌蜱的存活率，仅对其繁殖能力产生有限影响。基于微生物组、非靶向代谢组和转录组分析，证实长角血蜱具有复杂且高效的高温胁迫修复机制。其中，长角血蜱的内共生菌类考克次氏体（*Coxiella*-like endosymbiotic of *H. longicornis*，CLE-Hl）和热激蛋白 68（*heat shock protein 68*，*Hsp68*）基因在长角血蜱高温耐受中发挥了关键作用。综上所述，本研究从多组学层面揭示了长角血蜱的高温耐受机制，并进一步证实长角血蜱具有良好的生态适应性。

关键词

长角血蜱; 短暂极端高温胁迫; *16S rRNA* 高通量测序; 转录组学; 非靶向代谢组学